Master thesis and internship[BR]- Master's thesis : Experimental Procedure for Measuring the Noise Annoyance from Multi-Rotor Maneuvers using a UAV System[BR]- Integration Internship

Auteur : Beaulieu, Guillaume
Promoteur(s) : Dimitriadis, Grigorios; 15830
Faculté : Faculté des Sciences appliquées
Diplôme : Master en ingénieur civil en aérospatiale, à finalité spécialisée en "aerospace engineering"
Année académique : 2021-2022
URI/URL : http://hdl.handle.net/2268.2/13877

LIÈGE université
School of Engineering

von KARMAN INSTITUTE
FOR FLUID DYNAMICS

Experimental Procedure for Measuring the Noise Annoyance from Multi-Rotor Maneuvers using a UAV System

Master's thesis carried out to obtain the degree of Master of Science in Aerospace Engineering

Guillaume Beaulieu 152805

University of Liège - School of Engineering and Computer Science

Supervisors
Pr. Grigorios Dimitriadis
Pr. Christophe Schram

Advisor
Ir. Erica Gallo

Academic year
2021 - 2022

Acknowledgments

Tout d'abord j'aimerais remercier mes parents qui m'ont offert la possibilité de suivre ces études mais aussi et surtout encouragé durant ces années. J'aimerais aussi remercier ma famille, mes amis et ma petite amie qui m'ont soutenu et sans lesquels je n'aurais pas passé de si belles années en tant qu'étudiant.

Ensuite je remercie toute l'équipe du département de Dynamique des Fluides Environementales et Appliquées et particulièreemnt la section Aéroacoustique de l'Institut von Karman pour leur acceuil mais surtout pour leur disponibilité et aide précieuse. Un merci tout particulier à Erica Gallo pour son aide tout au long du projet.

Je remercie tout particulièrement mon promoteur Christophe Schram qui m'a suivi et aidé durant ce quadrimestre pour sa disponibilité ainsi que pour m'avoir transmis ses connaissances en aéroacoustique.

Enfin je remercie mon promotteur académique Grigorios Dimitriadis pour le suivi le long de mon master et toutes ses remarques intéressantes sur mon projet.

First of all I would like to thank my parents who offered me the possibility to follow these studies but also and especially encouraged me during these years. I would also like to thank my family, my friends and my girlfriend who supported me and without whom I would not have spent such great years as a student.

Then I would like to thank the whole team of the Department of Environmental and Applied Fluid Dynamics and especially the Aeroacoustics section of the von Karman Institute for their welcome but mainly for their availability and precious help. A special thanks to Erica Gallo for her help throughout the project.

I particularly thank my supervisor Christophe Schram who followed me and helped me during these last four months for his availability as well as for having transmitted his knowledge in aeroacoustics to me.

Finally, I thank my academic supervisor Grigorios Dimitriadis for the follow-up along my master and all his interesting remarks on my project.

Guillaume Beaulieu
Liège, January 5th 2022

Abstract

Nowadays, drone deliveries and urban air mobility are in conception and would arrive in our lives in the near future. These firsts are more often multi-rotor VTOL UAVs. This configuration is designed in order to operate in urban environments. The drones are likely to expose regularly to communities significant levels of noise. At the moment, no acoustic regulation exists to decrease the impact of disturbance in populated areas. However, the purpose of this research is to obtain a first understanding of the noise produced by a sUAV and on the impact on observers in the surroundings. Acoustic measurements of a sUAV multi-rotors have been performed in a free environment on the campus of the von Karman Institute for Fluid Dynamics. The recordings were conducted when the drone was hovering, flying over, tilting and in transition. The processing of the pressure data was focused on the power spectrum, the spectrogram and on three Sound Quality Metrics in order to give an evaluation of the noise annoyance.

The power spectra and the spectrograms reveal that for all maneuvers except the hover, the main BPF peak takes a larger range of frequencies and these lasts are varying because of the varying rotational speed of the front and rear propellers. Also, they show that over 3000 Hz, the tonal noise becomes hidden by the broadband one which becomes dominant.

Concerning the Sound Quality Metrics, they show that the overall Psychoacoustic Annoyance score is higher for the fly-over and transition maneuvers compared to the hovering flight. Therefore, the analysis with these different tools shows that the fly-over and the transition phase are the more annoying maneuvers for the human ear and have a greater impact on the community.

Acronyms

B

BPF : Blade Passing Frequency
BVI : Blade Vortex Interaction
BWI : Blade Wake Interaction

D

DAQ : Data Acquisition System

F

FFT : Fast Fourier Transform

J

JAFAAR : Jet Aeroacoustic Facility for Aeronautical and Aerospace Research

P

PSD : Power Spectral Density

R

RMS : Root Mean Square
RPM : Revolutions Per Minute

S

SD : Standard Deviation
SPL : Sound Pressure Level
SQM : Sound Quality Metrics

U

(s)UAV : (small) Unmanned Aerial Vehicle

V

VKI : Von Karman Institute for Fluid Dynamics
VPS : Vision Positionning System
VTOL : Vertical Take-Off and Landing

Contents

1 Introduction

Unmanned Aerial Vehicles (UAV), also called drones, will be part of our daily life in a very short future due to the wide range of applications they can imply. They can be used for photography, pipes or wind turbines inspection, package delivery but also in the future for passenger transport. These utilities cover each sort of area and range from grasslands to cities passing by mountains. Therefore the noise produced by these drones, which did not exist before, need to be tolerated by the civilization. Hence, these vehicles are known to be particularly annoying in terms of noise.

In this framework, Christian and Cabell [1] conducted psychoacoustic experiments comparing the sound produced by typical vehicles and by small UAV (sUAV) in residential communities. At equivalent metrics levels, their results led to the subjects being more disturbed by the noise of the sUAV than by ordinary road vehicles. Torija *et al.* [2] also measured the noise generated by a small quadcopter and found that the frequency spectra in low to mid-range is dominated by multiples tones as Blade-Passing Frequency (BPF) and its harmonics. But in the higher range, the electric motors also generates an important source of noise as high-frequency tones. In addition to humans, wildlife can be impacted by drone noise. For example, researchers and park rangers observed signs of disturbance among elephants when they used a UAV system to track these animals in Gabon, Africa [3].

However, the use of drones could drastically decrease working costs and should be a potential asset for delivery companies [4]. Also, drones would permit to reduce urban congestion and pollutants in urban areas. But apart the problem of noise acceptance, the main concerns are the safety and the personal living environment violation [5]. As a matter of fact, the zones where the drone will have the highest added value are the urban or more populated areas. A study reveals that drones have a good potential for high priority deliveries (for the medical sector for instance) in a short term. Nevertheless, drones used for food or clothes deliveries would not be accepted by the population in the long term [6, 5]. Therefore, silent drones begin to be a necessity.

The noise produced by a UAV depends on the model, the payload and the flight conditions [7]. Several maneuvers have already been studied such as the hovering flight and the fly-over [8]. The transient phase phenomena, however, involves fast variations of the noise level and in frequencies. It induces more attraction and dislike by the human communities. In addition to these variations, the annoyance for the human ear can also be evaluated with some Sound Quality Metrics (SQM). Torija *et al.* [2] performed a simple pass-by with quadcopters to compare their SQM with the road vehicles' ones. It has been found that the loudness, tonality and sharpness from the drone were higher compared to the ones from the road vehicles and aircraft. This last higher SQM, the sharpness, is principally due to the high intensity of high frequencies in the drone noise.

Consequently, the main goals of current researches are to find new types of noise assessments, methods and metrics to evaluate the noise impact on the community in order to optimize the design and operation of novel aerial vehicles. Waiting for this, the development of drones utilities could be thought by concentrating the flights paths along busy main roads to reduce the negative impacts of the noise on the public [5].

Research project

The issues stated above lead to the main topics of this Master's thesis. This research project focuses first on the way to measure the noise properly in a free environment. Then, it centers on the spectral analysis of different maneuvers such as the hover, fly-over, tilting and transition. The last research question concerns the noise annoyance produced by the most common flight maneuvers of a small quadrotor Unmanned Aerial Vehicle in a free environment. Therefore the objective of this study is to compare the noise produced in hovering flight, in a forward free-flight and in a transition phase.

This thesis is split up into chapters. In the second one, a theoretical background is provided in order to understand the methodologies used to discuss the results. In this chapter, a brief explanation is made about the aerodynamic noise. Then, the different sorts of graphs are explained to process the recorded pressure data. Next comes an introduction to psychoacoustics and noise annoyance. The final part of this chapter focuses on the theory about the noise sources produced by the rotating blades.

The third chapter deals with the experimental set-up used to record the sound and the methodology followed. The employed sUAV is introduced first. It is followed by the microphones types and the data acquisition. Then the two zones of recording, the anechoic chamber and the free environment, are described. The chapter finishes with the maneuvers performed during the recordings and is discussed in the next one.

Finally, the fourth chapter talks about the results obtained by recording the sound pressure of the drone flying in different configurations. But before, sound assessments are performed in order to check if the executed measurements are properly made. The different methodologies, explained in the theoretical background such as the spectra, spectrograms and sound quality metrics, are used to present the four drone maneuvers noise. This chapter finishes with a comparison of these different flight configurations.

2 Theoretical background

Throughout this chapter, the required concepts will be explained with their applicability to this research. First, the general aspects of aerodynamic noise are clarified. Secondly, the theory about the different analysis methods is developed. Then, notions of psychoacoustics and sound quality metrics are defined. Finally, the concepts on the drone and rotating blades noise are discussed.

2.1 Aerodynamic sound/noise

The sound is a vibration that propagates through a transmission medium as a pressure wave. The equation used to describe the homogeneous wave motion in absence of any source is defined in Equation (2.1). The audible frequency range for humans stands between 20 Hz and 20 kHz. In the air, these frequencies represent sound waves with a wavelength between 17 m and 1.7 cm.

$$\frac{1}{c_0^2}\frac{\partial^2 p'}{\partial t^2} - \nabla^2 p' = 0 \tag{2.1}$$

Where $\nabla^2 := \Delta$ the 3-dimensional Laplacien, p' the pressure perturbation, t the time and c_0 the propagation velocity of the wave (343 m/s for the sound in the air at 20°C).

But sound sources can be more accurately described as monopoles, dipoles and quadrupoles, as defined below [9].
A monopole can be seen as a pulsating sphere, contracting and expanding with time. In other words, this is a point source that radiates equally in all directions. The monopole is the simplest type of source and is used as a build-up component for more complex sources such as dipole and quadrupole.
By definition, a dipole source can be seen as an oscillating sphere or as two small adjacent spheres (monopoles) that are pulsating exactly out of phase. They are due to a variation of momentum fluxes with time.

A quadrupole can be seen as a deforming sphere without change of volume nor net force. It can be seen as two dipoles or four monopoles with altering phases at the corner of a rectangle.

On the other hand, the noise can be defined as a non-desirable sound and as a nuisance. Therefore as the sound produced by a drone is shown to be annoying for the human ear [10, 7], the term "noise" will be mostly used along this thesis.

2.2 Pressure signal processing methods

All the pressure data recorded by the microphones have to be processed in order to be analyzed correctly. The first method is to compute the root mean square (RMS) of the time signals recorded. This method will be used to determine the position of the drone in the microphones' square with time (schematized in Figure 3.2). Then, the Power Spectral Density (PSD) analysis is performed. This kind of graph will show the dominant frequencies and it will help to distinguish the different noise source mechanisms. Finally, the spectrogram will be used. The latter is useful to check the frequencies involved and dominant along time. These frequencies are computed with Fast Fourier Transform but for small time segments to obtain time-varying frequencies.

Root mean square

The root mean square (RMS), of a signal is defined as the process used to determine the average power output over a long period of time. The RMS is computed as

$$x_{\text{RMS}} = \sqrt{\frac{1}{n}(x_1^2 + x_2^2 + ... + x_n^2)} \tag{2.1}$$

in the case of a set of n values.

RMS values give a way to describe how noise signals combine. However, for a continuous sound, the standard deviation analysis is preferred to have the mean in the calculation. Therefore, the standard deviation is a measure that is used to quantify the amount of variation of a set of data values. In other words, a small standard deviation indicates that the values stand close to the mean of the set and a high standard deviation means that the data are spread out over a wider range of values. The standard deviation of the data is computed as:

$$\text{SD}_i = (x_i - \mu)^2 \tag{2.2}$$

where

$$\mu = \frac{1}{n}\sum_{i}^{n} x_i \tag{2.3}$$

is the mean of the signal.

Power Spectral Density Analysis

A sound spectrum is a representation of a sound. It presents the different vibration frequencies present in this sound. It is presented as a graph of power or pressure as a function of frequency. The power or pressure is measured in decibel and the frequency in vibrations per second or Hertz.

The Power Spectral Density (PSD) computation is described as follows. First, the signal is cut into several segments which are lightly overlapped. Then a windowing of each segment is performed in order to compute the Fourier Transform of these firsts. Finally, the mean of the results is calculated. This methodology is schematized in Figure 2.1.

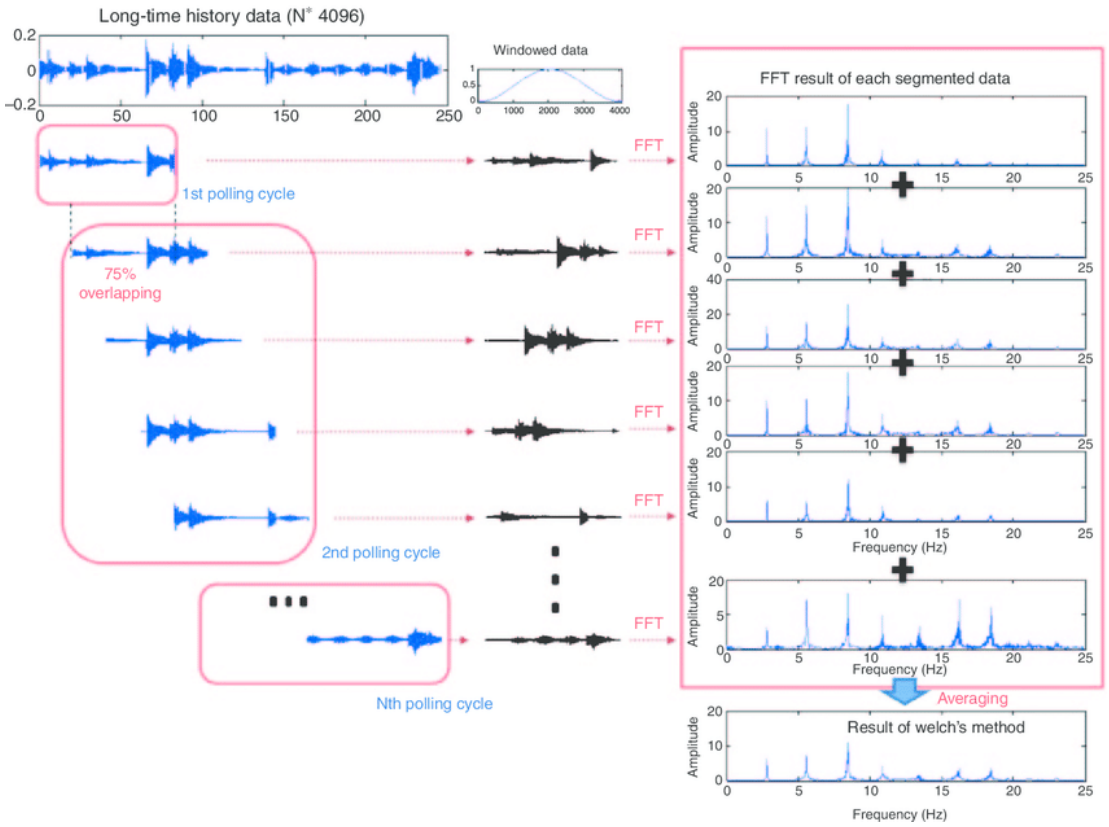

FIGURE 2.1: Example of the segments splitting and on the FFT computation of each segment to make the mean. Image from [11].

To compute it, the function *scipy.signal.welch* on Python is used (as shown in Appendix A). It takes the pressure data as an input to give the different frequencies present in the recorded sound. Welch's method is chosen instead of the Fast Fourier Transform (FFT) because, as explained, this first slices the original signal in several pieces and averages the spectra of these ones. It permits a reduction of the noise in the signal. The price to pay for averaging is to obtain less narrow peaks as the FFT would give. This compromise is schematized in Figure 2.2.

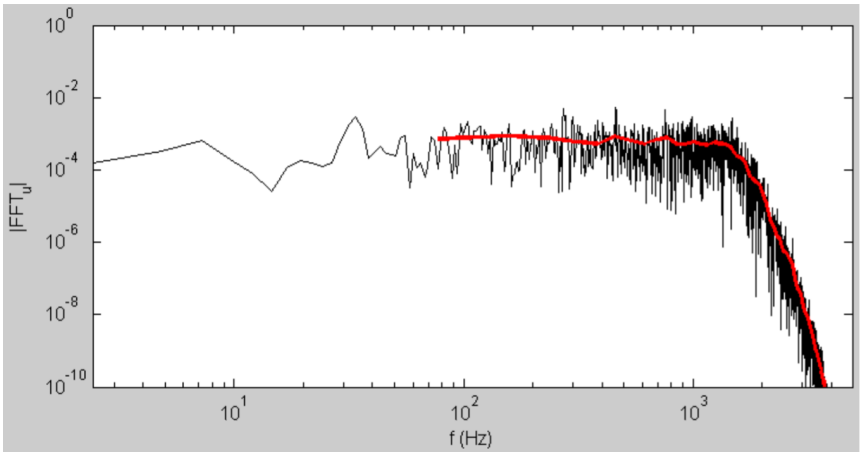

FIGURE 2.2: Spectral analysis of an example signal computed with the Fast Fourier Transform in black (full length signal of 4096 pts) and with the Welch's method in red (average of 32 FFTs of signal segments, 128 pts each). Image from [12].

The mathematical definition of this method is therefore: A signal of length M is split in K segments of length N and separated at D point to each others. The k^{th} segment is written $X_k(n) = x(n + (k-1)D)$. The estimation of the Welch's PSD $\hat{S}_{\text{Welch}}(\omega)$ is defined in Equation (2.4).

$$\hat{S}_{\text{Welch}}(\omega) = \frac{1}{KNU} \sum_{k=1}^{K} \left| \sum_{n=1}^{N} h(n) x(n + (k-1)D) \exp(-j\omega n) \right|^2 \tag{2.4}$$

where $h(n)$ is a weighting window of length N and U is the weightings normalization constant insuring that $\hat{S}_W(\omega)$ is asymptotically biased. This last is defined as

$$U = \frac{1}{N} \sum_{n=1}^{N} |h(n)|^2 . \tag{2.5}$$

Spectrogram by Fast Fourier Transform

Along this thesis, the spectrogram will be used to analyze the sound produced by the drone. This kind of graph is a visual representation of the spectrum of frequencies of a signal varying with time. The methodology to plot a spectrogram is first: dividing the signal with a small time step into time segments (which are overlapping by taking some points of the neighboring segments). With these smaller time signal segments, a separate discrete FFT is performed in order to define the frequencies involved. Finally, with all the frequencies obtained for each time segment, they are put side by side and an interpolation is added between them. This is computed with the function *matplotlib.pyplot.specgram* in Python as shown in Appendix B.

The mathematical definition of the discrete Fast Fourier Transform for a signal s of N samples is written in Equation (2.6).

$$S(k) = \sum_{n=0}^{N-1} s(n) \exp\left(-2i\pi k \frac{n}{N}\right) \quad \text{for} \quad 0 \leq k < N. \tag{2.6}$$

2.3 Psychoacoustic/Noise annoyance metrics

Several methods exist to quantify the effect of noise. The most common is the Sound Pressure Level (SPL). However, there are other metrics known as *loudness*, *sharpness* and *roughness* which are used to measure the "Sound Quality".

Sound pressure level

A basic way to express the sound level of an acoustic signal is through the Sound Pressure Level. The values are expressed in decibel (dB). It is a common value and this metric will be used all along this thesis. The SPL is computed as:

$$SPL = 10 \log_{10} \frac{p_{\text{rms}}^2}{p_{\text{ref}}^2} \tag{2.1}$$

where the reference pressure p_{ref} is the pressure at the threshold of the human ear and equal to 20µPa and the root mean square pressure p_{rms} corresponds to the time-averaged square of the pressure fluctuation. In fact, if $p(t)$ is the pressure of the fluid at a point, the pressure fluctuation is defined as $p'(t) = p(t) - p_0$ with p_0, the mean background pressure. Therefore, one can write:

$$p_{rms} = \sqrt{\frac{1}{2T} \int_{-T}^{T} (p(t) - p_0)^2 dt}, \tag{2.2}$$

where T is the integration period which is large enough to include all the frequencies in the signal.

Along this thesis, p_{rms} is equal to the square root of the Welch's PSD $\hat{S}_{\text{Welch}}$ computed as explained in the precedent subsection and shown in Appendix A.

Sound quality metrics

Sound Quality Metrics (SQM) have been computed with MoSQITo [13], a python code, developed by acoustic engineers to provide an objective assessment of the pleasantness of a sound.

The calculation of some sound quality metrics are included in major commercial acoustic and vibration measurement and analysis software. However, some of the proposed metrics result from in-house implementation and can be dependent on one system to another. Some implementations may also lack of complete documentation and validation on publicly available standardized sound samples.

Loudness: Loudness, measured in sone, is the subjective perception of sound pressure. It can be defined as: "That attribute of auditory sensation in terms of which sounds can be ordered on a scale extending from quiet to loud" [14]. The acoustic loudness calculation from the Zwicker method was firstly introduced for steady signals [15]. Afterwards, it has been extended to non-stationary sounds (DIN 45631, 2010) and the method is still in accordance with ISO 226:1987. In MoSQUITo, the code is based on the C++ program published with ISO 532-1(2017) [15].

Sharpness: Sharpness is a measure of the high-frequency content of a sound. In other words, the greater the proportion of high frequencies, the sharper the sound. Zwicker and Fastl [16] have defined a sound of sharpness 1 acum as "a narrow band noise one critical band wide at a center frequency of 1kHz having a level of 60dB". Also, the acoustic sharpness was introduced as a standard in the DIN 45692 [17] and this 'din' weighting function is used in MoSQUITo (based on the standard published in 2009). The calculation of the sharpness is based upon the specific loudness distribution of the sound. As explained in the previous paragraph, the loudness is calculated according to the Zwicker's method.

Roughness: Roughness is a complex acoustic effect that quantifies subjectively the perception of rapid (15 to 300 Hz) amplitude fluctuation of a sound. Its unit of measure is the asper and it is defined as: "One asper is defined as the roughness produced by a 1000Hz tone of 60dB which is 100% amplitude modulated at 70Hz " [16]. However, no standardization is already official. Several models have been developed to compute the roughness and the one used in MoSQUITo is based on the algorithm described in Daniel and Weber (1997) [18]. Also, some reference values for the roughness of amplitude-modulated tones are proposed by H.Fastl and E.Zwicker [19].

2.4 Noise sources by rotating blades

Rotating blades emit two distinct types of acoustic signature. The first one refers to an harmonic noise, or a tone caused by sources that repeat themselves at each rotation (Figures 2.3 and 2.4). The second one is the broadband noise which is caused by turbulent effects around the blades. The latter is shown in Figure 2.6. Finally, Figure 2.7 illustrates these signals and shows how they combine [20].

Tonal noise

The tone, also called the harmonic noise, is generated by rotating equipment at a predictable frequency relating to the rotational speed of the rotor. The fundamental tone may also manifest itself by progressively lower intensity levels at integer harmonic multiples.

The signature of a single-bladed rotor during one period of revolution T_p is shown in Figure 2.3 and if the rotor has three blades (Figure 2.4), its signature is repeated at the blade-passing frequency (BPF) which correspond to $T_p/3$. The different source mechanisms of tonal noise are explained below.

Thickness noise: Thickness noise can be seen as a monopole [21]. It depends only on the shape and the motion of the blade. This noise is caused by the displacement of the air by the rotor blades. This type of noise is not dominant for a UAV due to the small size of the blades. In addition, thickness noise is primarily directed in the plane of the rotor (as shown in Figure 2.5 [22]).

Loading noise: The second source is the loading noise. This latter can be represented as a dipole [21]. It is represented as an aerodynamic effect due to the acceleration of the force distribution on the air around the blade by passing through it. This type of noise is primarily directed below the rotors as schematized in Figure 2.5.

Blade vortex interaction: Then, the Blade Vortex Interaction (BVI) noise is mostly present in hover flight since it is generated by the interaction of the shed tip vortex with the following blade.

Blade wake interaction: Finally, the turbulent wake following the previous blade induces a Blade Wake Interaction (BWI) noise by interacting with the next one.

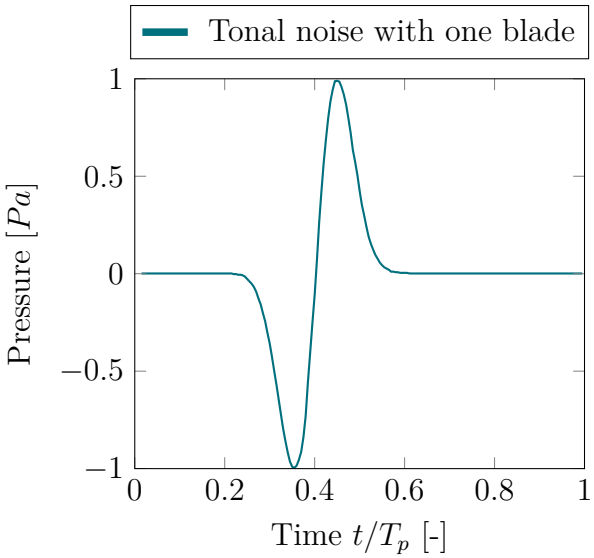

FIGURE 2.3: Tonal noise with time for a single blade rotor during the period of one revolution T_p [20]

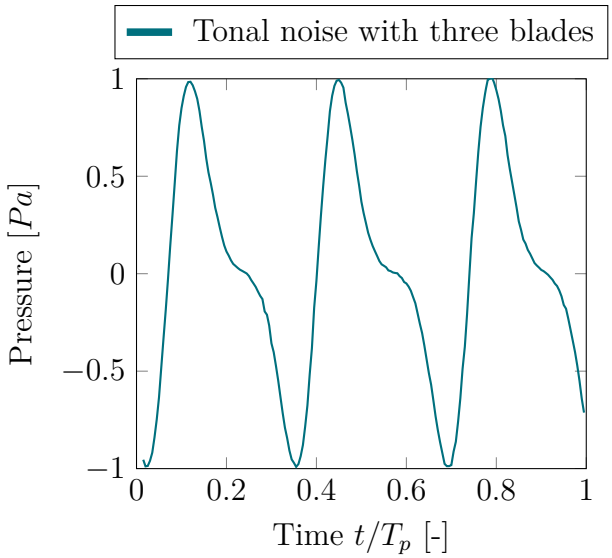

FIGURE 2.4: Tonal noise with time for a 3 bladed propeller during the period of one revolution T_p [20]

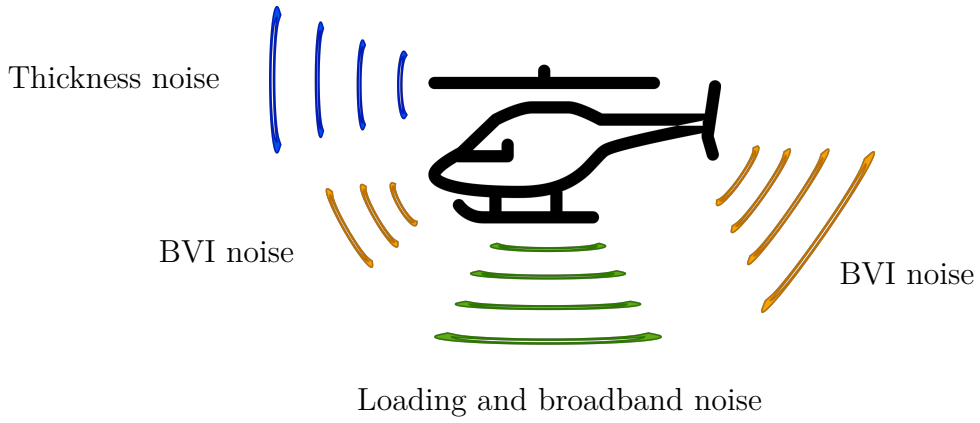

FIGURE 2.5: Direction of propagation of the noise from a rotating blade[22, 23]

Broadband noise

The broadband noise occurs generally in higher frequencies and can be seen as a dipole or a quadrupole [24]. This noise is generated by load fluctuation due to inflow turbulence, tip vortices formation, boundary layers passing the blades trailing edges and different turbulence contributions. In other words, broadband rotor noise is always caused by random variations in blade loading resulting from the interaction of the blades with turbulence. Figure 2.6 illustrates a typical broadband noise. This signal, compared to the tonal one, has no associated periodicity but an envelope that varies periodically. Figure 2.7 shows the sum of the two signals and this sum is dominated by the tonal noise.

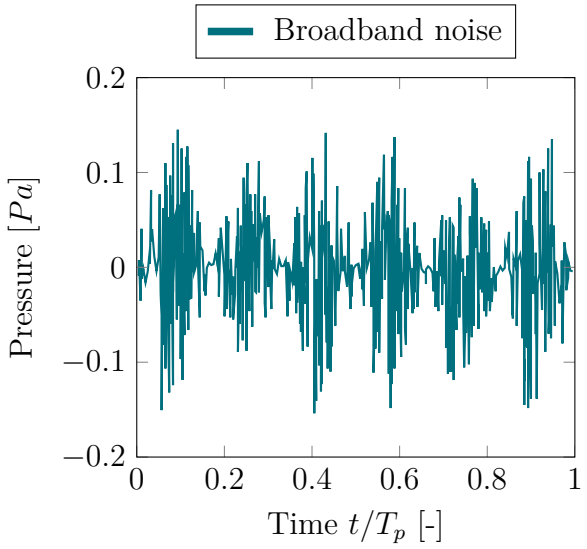

FIGURE 2.6: Broadband noise produced by a rotor [20]

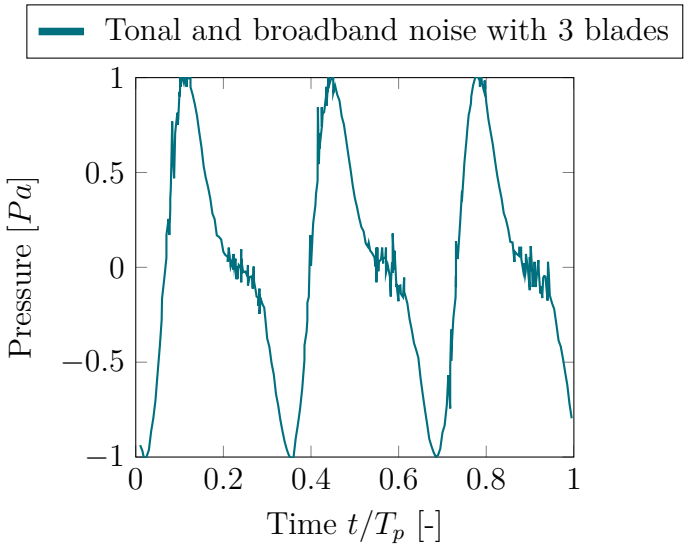

FIGURE 2.7: Tonal and broadband noise combined for a 3 bladed rotor [20]

Computation of the Blade-Passing Frequency

The Blade-Passing Frequency (BPF) is a pure tone produced by the rotor. This analysis is important to distinguish the tonal and the broadband noise and it permits to determine the most important noise source mechanisms. As it has been seen higher in this section in Figure 2.4, the sound mechanism is tonal and the peaks are emitted at the BPF and its harmonics. The BPF (in Hz) is defined as

$$f_{\mathrm{BPF}} = \frac{B\Omega}{60} \tag{2.1}$$

where B is the number of blades and Ω the rotational speed in revolutions per minute (rpm). An example of these tonal peaks is observed in Figure 2.8, a typical noise of a 3-bladed rotor at 600rpm [20]. The tone noise is defined by the peaks which occur at the blade-passing frequencies at a multiple of 30 Hz. At higher frequencies, the broadband noise becomes dominant on the spectrum.

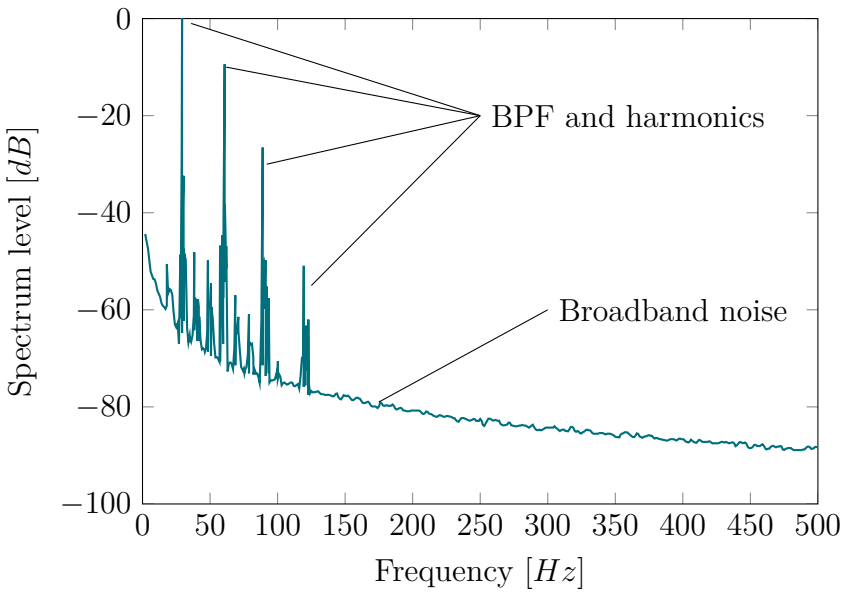

FIGURE 2.8: The spectrum of the rotor noise showing harmonics at blade-passing frequency and broadband noise for a three-bladed rotor turning at 600 rpm. The blade-passing frequency $f_{\mathrm{BPF}} = 30$ Hz [20]

Electric motor noise

The electric motors used to rotate the propellers produce also an important source of noise in the form of high frequency tones [2]. This noise depends on the RPM of the propellers. For the drone used for this study, the DJI Phantom 3 SE, the model of the electric motors are the DJI 2312 (shown in Figure 2.9) and the frequencies of the noise

FIGURE 2.9: Electric motor of the drone DJI Phantom 3 SE: 2312 [25]

produced in steady flight stands around 3500 and 5100Hz [26]. These two peaks produced by the electric motor can be seen on each spectrum in the sections in Chapter 4.

3 Experimental setup

Through this chapter, the explanation of the equipment used to perform the experimental campaign based on the noise emissions of a maneuvering drone is introduced. Then the recording areas are described. And finally, the different maneuvers measured are explained.

3.1 Drone and flight instrumentation

The DJI Phantom 3 SE, shown in Figure 3.1, was used for this study. This drone is a famous recreational UAV used to record videos and take photographs. It has a maximal speed of 16 m/s and maximal ascend and descend speeds of 5 and 3 m/s respectively. The drone has four two-bladed propellers and it has a weight of 1236 g. The intelligent flight battery lasts approximately 25 minutes in hovering flight.

FIGURE 3.1: Drone DJI Phantom 3 SE [27]

The drone has a GPS used for its positioning. Moreover, different sensors are also installed on the drone. It is equipped with a Vision Positioning System (VPS) including one molecular camera and two ultrasonic sensors. This system is used when the drone is flying in an indoor environment when the GPS system is unavailable. The DJI VPS helps the aircraft to maintain its current position.

3.2 Microphone and data acquisition

Four microphones Gras 40PL (shown in Figure 3.4) were used to measure the noise induced by the drone. The microphones are positioned like a square of 2.3m side and at a height of 1.2m, as it can be seen in Figures 3.2 and 3.3. They are pointing to the center of the square, where the drone is flying.

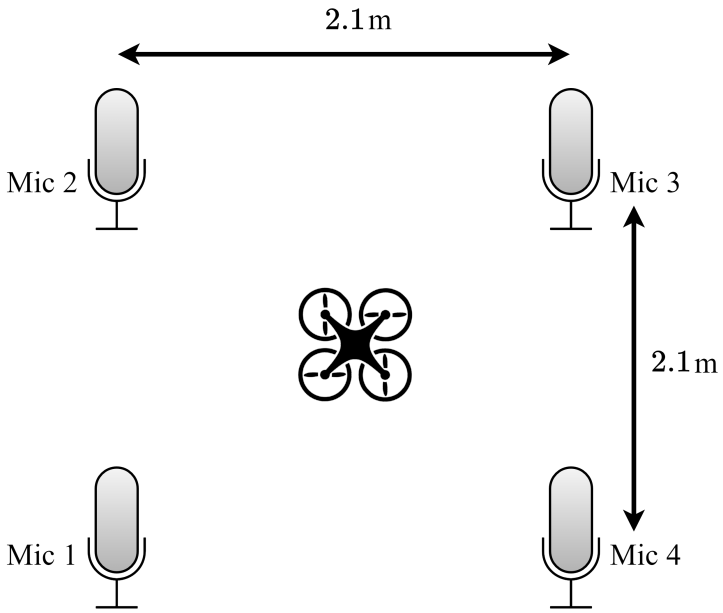

FIGURE 3.2: Position of the microphones and the drone in the center [23]

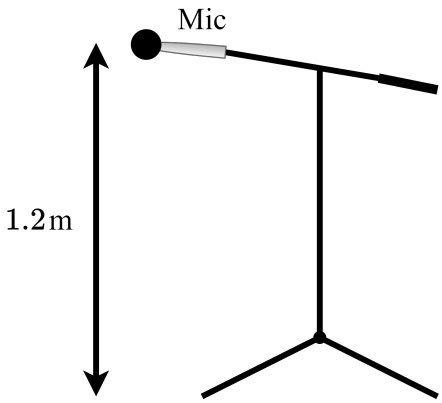

FIGURE 3.3: Height of the microphones

They have been chosen because they are array microphones. This type of microphone has the characteristic of being phase-matched.

They have a length of 59.1 mm and a diameter of 7.0 mm. The microphones present a frequency range from 10 Hz to 20 kHz. Therefore by the Nyquist sampling theorem, the sampling frequency for the acquisition was set to a frequency of 51,200 Hz to avoid aliasing. The 40PL-10 has a dynamic range from 33 dB(A) to 147 dB peak, the upper limit is the peak value before visible clipping. The microphones have been calibrated with a pistonphone calibrator (shown in Figure 3.5) and they have a sensitivity of 10mV/Pa. The instruments were centralized to the Data Acquisition System (DAQ) which was connected to a laptop equipped with LabView [28] in order to record the pressure variation.

FIGURE 3.4: Microphone Grass 40PL [29]

FIGURE 3.5: Pistonphone calibrator Brüel & Kjaer type 4231 [30]

3.3 Anechoic chamber: JAFAAR

The experimental campaign has been partially carried out in an anechoic chamber for indoor sound measurements of the drone system. More in detail, the facility available at the von Karman Institute (VKI) is named Jet Aeroacoustic Facility for Aeronautical and Aerospace Research (JAFAAR). The latter was mainly designed for the jet acoustic studies whilst accommodating a free-jet test section. However, as the jet setup can be easily removed, the facility can also allow noise measurements alone. The anechoic chamber dimensions are (4x3x4) m^3 and it has a cut-off frequency of 150 Hz [31]. Figure 3.6 shows the experimental setup used in the facility for the test campaign. As explained in Section 3.2, the microphones were placed as a square in order to record the sound emitted by the drone. The latter was manually controlled to fly in hover condition at around 1.8m above the ground. On the ground, a box covered with acoustic foam has been installed for the drone to take-off. In fact in absence of GPS signal in the chamber, the drone has a magnetic compass issue because of the presence of a metallic grid on the floor.

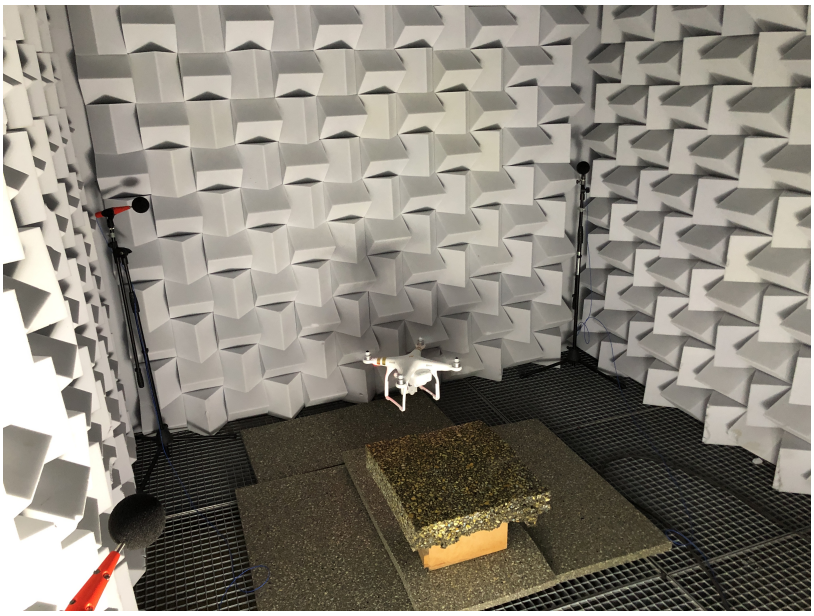

FIGURE 3.6: Anechoic chamber JAFAAR - von Karman Institute for Fluid Dynamics

3.4 Von Karman Institute: Outdoors

The same configuration of the microphones, introduced in Section 3.2, was used for the external measurements (as shown in Figure 3.7). In fact, in order to be able to compare indoor and outdoor sound emissions and to avoid discrepancies among the record data, it was necessary to keep the same distance from the ground of the microphones, as well as the same distance with respect to the flying drone.
The forecast during these experiments were

Temperature	Wind	Humidity	Pressure	Clouds	Floor
8°C	12 km/h	92%	1023 hPa	Few (10%)	Humid/Wet

TABLE 3.1: Forecast during the outdoors experiments. From windy.com

FIGURE 3.7: Outdoor experiments on the von Karman Institute's campus. The microphones are in a square configuration and connected to the acquisition system and to LabView on the PC.

3.5 Methodology: Flight maneuvers

The aim of the work was to understand the noise emissions of the DJI Phantom 3 SE whilst performing different flight maneuvers. In this perspective, an outdoor environment has no space limitations and it can allow the analysis of different flight conditions.

The first maneuver, performed inside JAFAAR as well as outdoors is the "hover" (shown in Figure 3.8). In other words, the drone is just flying at the same position and the more stable as possible. The campaign performed in the anechoic chamber was limited at this flight condition, given the space constraints. The hovering flight has also been used to

compare the interaction with the ground by varying the altitude of flying.
The fly-over, the tilting and the transition flight conditions were analyzed. A simple scheme of this first is shown in Figure 3.9. More in detail, the fly-over consists of moving forward at 2 m above the ground over the microphones at around 10 km/h.
For what concerns the tilting. This maneuver consists in flying rapidly back and forth between the microphones. It permits obtaining the noise emitted by the changing phases for a long time. This maneuver is schematized in Figure 3.10.
The last one called the transition, consists in flying forward at a constant speed, stopping between the microphones and going forward again as mapped in Figure 3.11. An additional view from the side is shown in Figure 3.12.

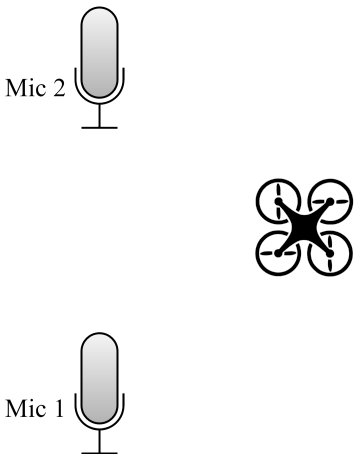

FIGURE 3.8: Scheme of the hover maneuver. Performed in JAFAAR and outdoors [23]

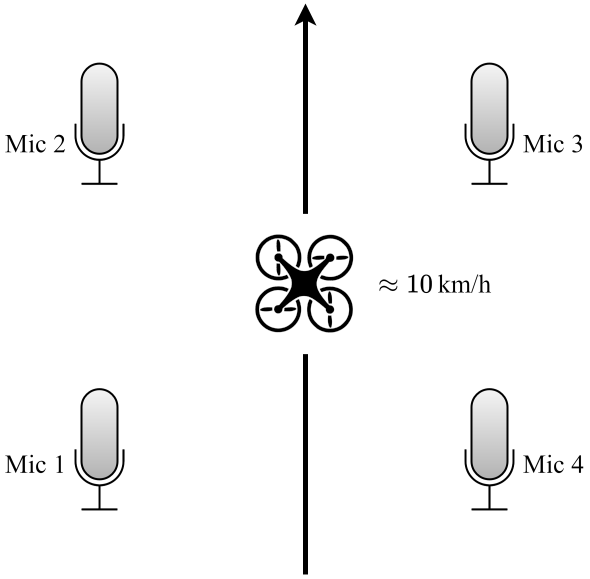

FIGURE 3.9: Scheme of the fly-by maneuver performed outdoors [23]

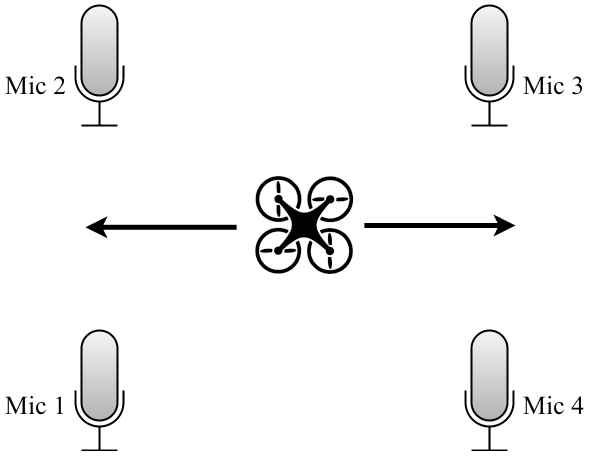

FIGURE 3.10: Scheme of the "tilting" maneuver performed outdoors [23]

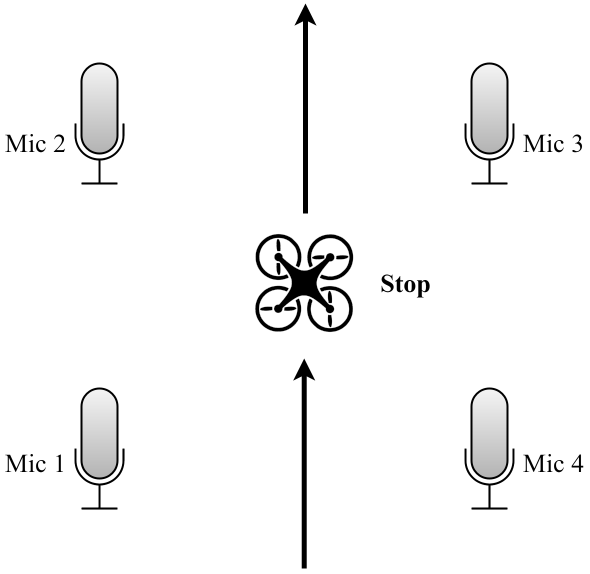

FIGURE 3.11: Scheme of the transient maneuver performed outdoors [23]

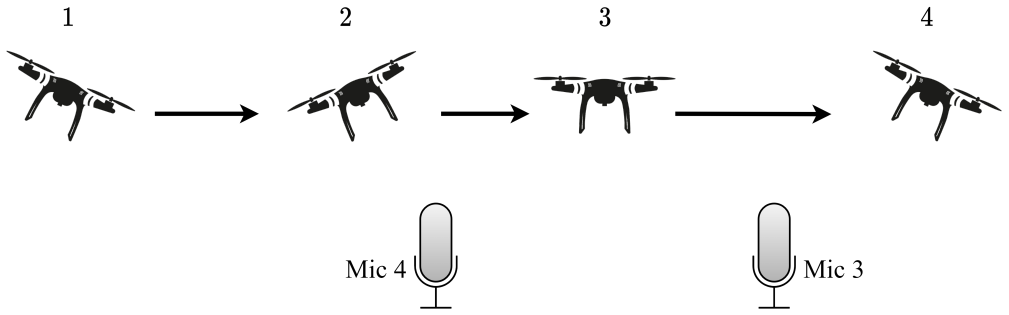

FIGURE 3.12: Scheme of the transient maneuver from the side. The different phases are: 1. Coming at a constant speed 2. Decelerating 3. Hovering 4. Accelerating forward [32]

4 Results and discussion

This chapter presents measurements previously described in Section 3.5. Initially, the sound assessment emitted during the hover condition is computed in the anechoic chamber. As a consequence, the hover emissions have been compared for indoor and outdoor environments. Furthermore, the results obtained for the different outdoor flight maneuvers are also discussed below. Finally, the psychoacoustic and noise annoyance analysis and their metrics, presented in Section 2.3, are discussed for these maneuvers.
During these tests, it was difficult to keep the drone exactly in the middle of the microphones' square. Then, the power recorded by each microphone was different depending on the distance between the drone and themselves. Therefore, the idea was to take a mean of the power spectrum of each microphone to obtain the most accurate value of the power in the center of the square.
For the spectrograms, only one microphone is taken into account because this method is dependent on time. In fact, if the drone is passing close to a microphone, it will distort the real value.
Finally, microphone 1 and microphone 3 will be analyzed for the psychoacoustic analysis. These two are on the left start and the other on the right end respectively.

4.1 Sound assessments

Noise between indoors/outdoors

The comparison of the noise emitted indoors and outdoors is a preliminary step for the understanding of the results. The matching of the sound emissions in both conditions is a significant aspect as it can allow assessing that no stronger effects of the atmospheric conditions are influencing the measurements. In this framework, as explained in Section 3.5, the easiest maneuver that can be performed to achieve this task is the hovering flight. As a matter of fact, if the pressure spectra show that the tonal peaks appear at the same frequency for indoor and outdoor tests, it can be asserted that the background noise

outdoors is negligible and the BPF is not affected. In fact, the idea to measure the sound emitted by the drone in an anechoic chamber is to avoid atmospheric disturbances.

Figure 4.1 represents the spectrum of the steady flight of the drone in the anechoic chamber JAFAAR in VKI. The noise produced by the drone outdoors is shown in Figure 4.2. The background recorded in the anechoic chamber remains high below 1000 Hz because turbomachinery experiments were taking place outside the room.

About the outdoor background noise and the recorded drone noise, it can be seen that the sound at low frequencies is not matching. It was due to a varying background noise coming from airplanes, cars or gardeners in the surrounding places. Nevertheless, it gives a good estimation.

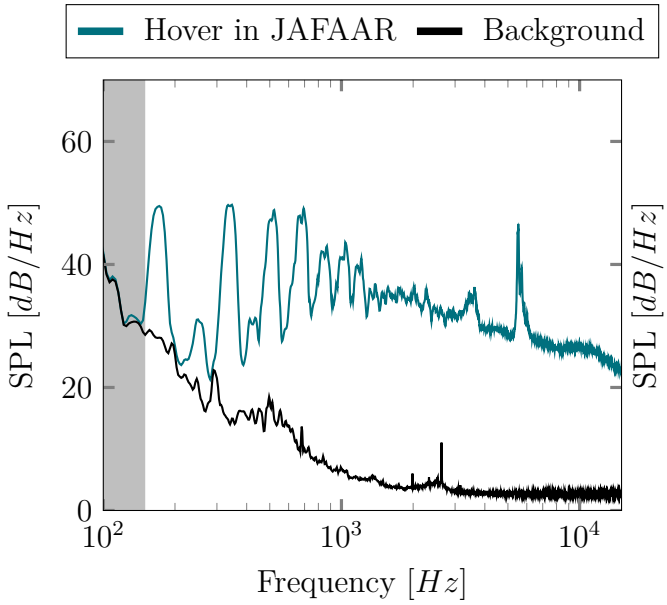

FIGURE 4.1: Spectrum of the hovering maneuver inside the anechoic chamber JAFAAR

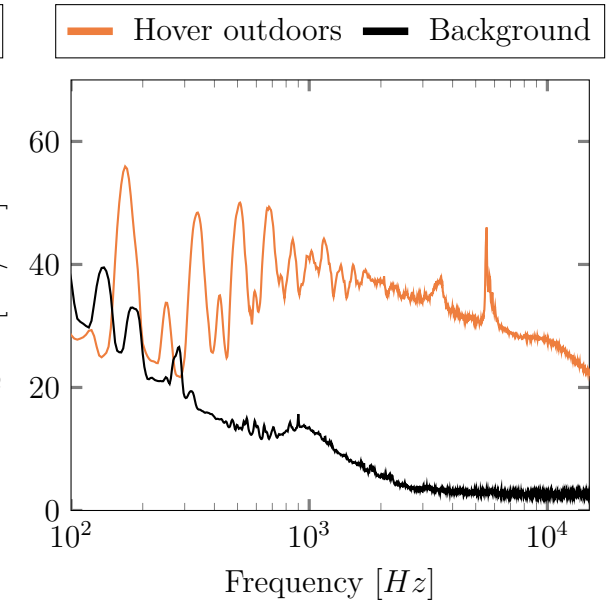

FIGURE 4.2: Spectrum of the hovering maneuver outdoors

With the spectrum obtained in Figure 4.1 or 4.2 and in the next sections, the computation of the main BPF can be carried out. This main BPF is the first peak appearing in the spectrum. The methodology is shown in Figure 4.3 and is explained below.

From passing by the spectrum in dB/Hz to a spectrum in Pa^2/Hz, the maximal value of the peak is taken (1). Then, the latest is divided by two and a horizontal line is drawn (2). The intersections of the line with the PSD are taken and the mean of these two is computed to find the main Blade-Passing Frequency (3). This method consists to have better accuracy in the computation of the BPF. In fact, by only taking the maximal value, the peak could not be well defined. The slopes are better.

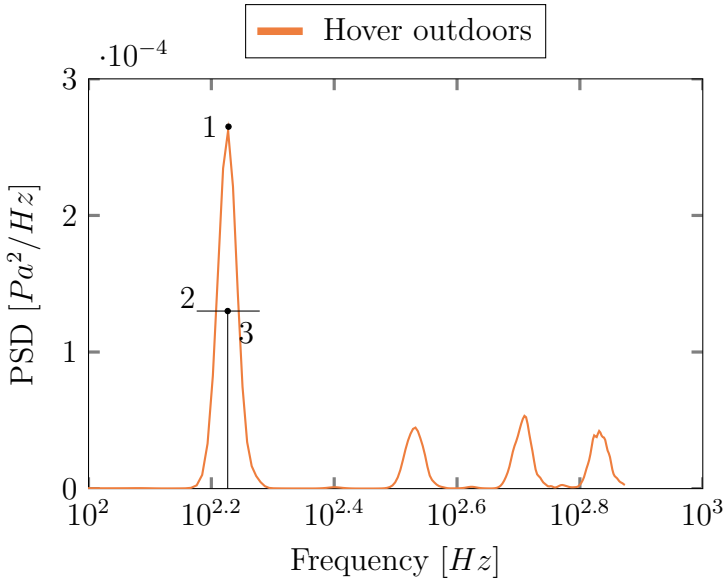

FIGURE 4.3: Example of computation of the main Blade-Passing Frequency with the spectrum of the hover flight performed outdoors. Here the BPF is 169 Hz.

By having the spectra of the same maneuver inside an anechoic chamber and outdoors, these should be compared in order to show the veracity of the results obtained in a free environment. The spectra are superposed in Figure 4.4.

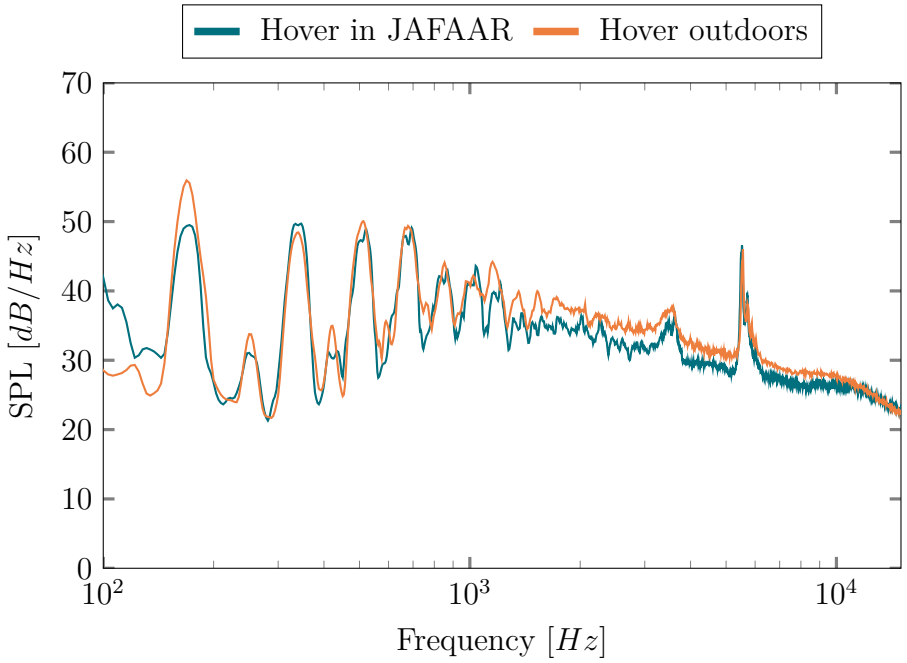

FIGURE 4.4: Difference of the spectra of the hovering maneuver between outdoors (BPF = 170 Hz) and inside JAFAAR (BPF = 171 Hz)

In this figure, it can be seen that the BPF and harmonics recorded are matching. This means that the frequencies measured in a free field are the same as the ones obtained in an anechoic chamber. However, the noise measured in the anechoic chamber JAFAAR appears to be lower in intensity. A possible explanation could be that over the basket-ball

field the sound can be reflected by the ground. This effect could lead to an increase in the measured levels.

Drone height

The drone height can affect the recorded sound. If the drone is too close to the ground, it can fly in its own wake and disturb the stability of this one and therefore varying the rotational speed of the propellers. Several assessment measurements of the hovering at different altitudes have been performed in order to avoid misinterpretations of the results.

The first measurement has been performed at 3m above the ground, so 1.8 m over the microphones.

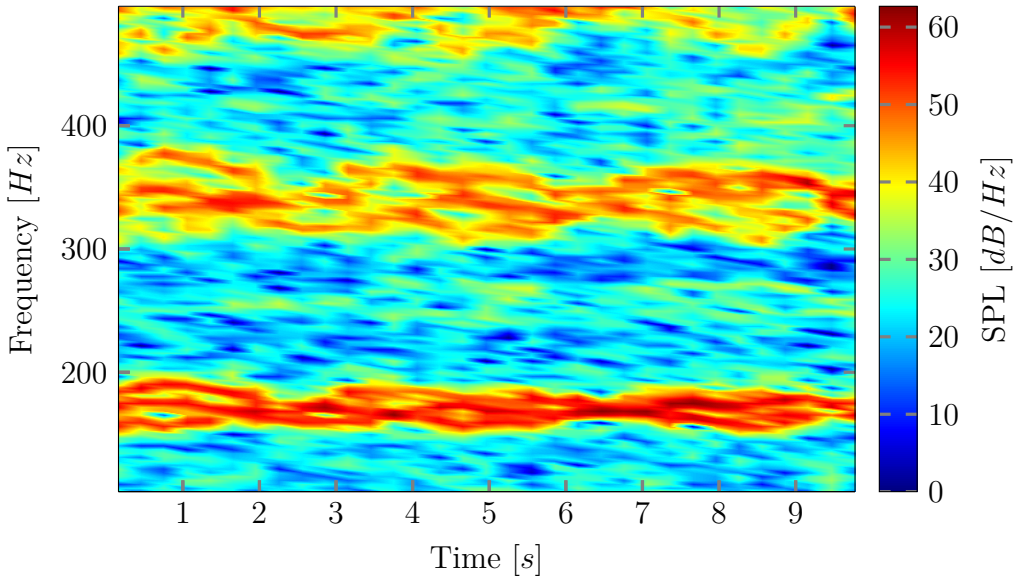

FIGURE 4.5: Spectrogram of the noise of the drone at 3m above the ground recorded by microphone 1

It can be seen in Figure 4.5 that the first BPF, calculated at the beginning of this Section, should be 170 Hz. However, in this graph along time, the first BPF is not well defined. The drone could be subjected to atmospheric turbulence which induces variations of the propellers rotational speed.

The second measurement has been performed at 1.8m above the ground, 60 cm above the microphones (Same recording as Figure 4.2).

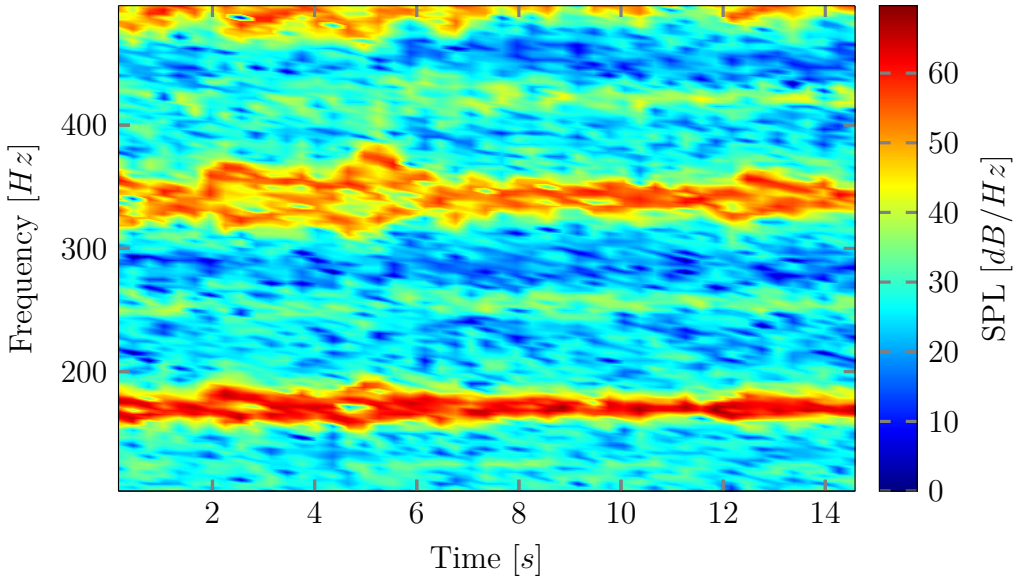

FIGURE 4.6: Spectrogram of the noise of the drone at 1.8m above the ground recorded by microphone 1

In this figure, the BPF at 170 Hz is well defined along time. The small perturbations/separations occurring at 3 and 5 seconds are due to a small wind and therefore, the automatic stabilization of the drone or a correction from myself to keep the drone in the center of the microphones' square. And instantly, it induces a changing of RPM of the different propellers.

The last measure has been taken at 50 cm above the ground. The spectrogram of this record is shown in Figure 4.7.

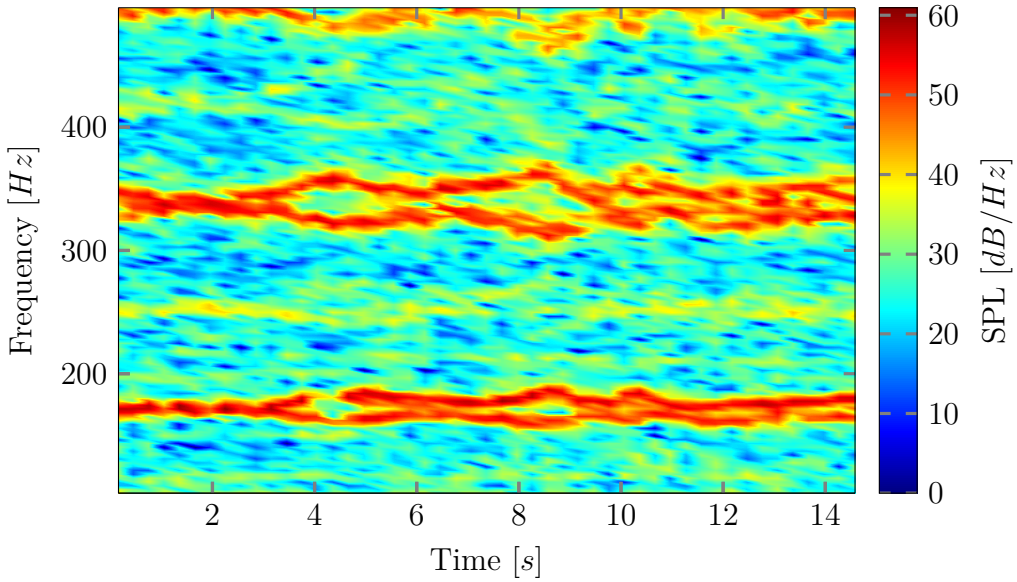

FIGURE 4.7: Spectrogram of the noise of the drone at 50cm above the ground recorded by microphone 1

In this graph, it can be noticed that the first BPF is not a line like in Figure 4.6 but two distinct lines.

Figure 4.7 shows the spectrogram of the drone hovering at 50 cm above the ground. It can be clearly seen that starting from 3 seconds, the BPF at 170 Hz is splitting in two. The separation is repeated at the first harmonic. This frequency split may be due to the difference in rotation speed of the rotors. Being a quadrotor, the stability of the drone is conducted by the thrust of the propellers. In this case close to the ground, the thrust induces wake and there may be some ground effect. These interactions would lead to instabilities that are compensated by the difference of thrust, and directly rotation speed, of the propellers.

With this analysis, it can be concluded that the drone height for the measurements needs to be performed around 1.8m above the ground. Therefore all the measurements and maneuvers performed along this thesis have been done at this height. The drone was flying at this height also in JAFAAR for the analysis in Figure 4.4.

Spectrogram of hover in JAFAAR

A little apart to show the variation of the frequencies of the hovering flight inside the anechoic chamber JAFAAR (same recording than Figure 3.6). The spectrogram shown in Figure 4.8 shows two frequency lines for the main BPF. This is mainly due to the small space where the drone was flying. As already mentioned in Section 3.6, the anechoic room is not big. It induced some wake and some propellers were rotating at higher speed than the other to stay steady in flight.

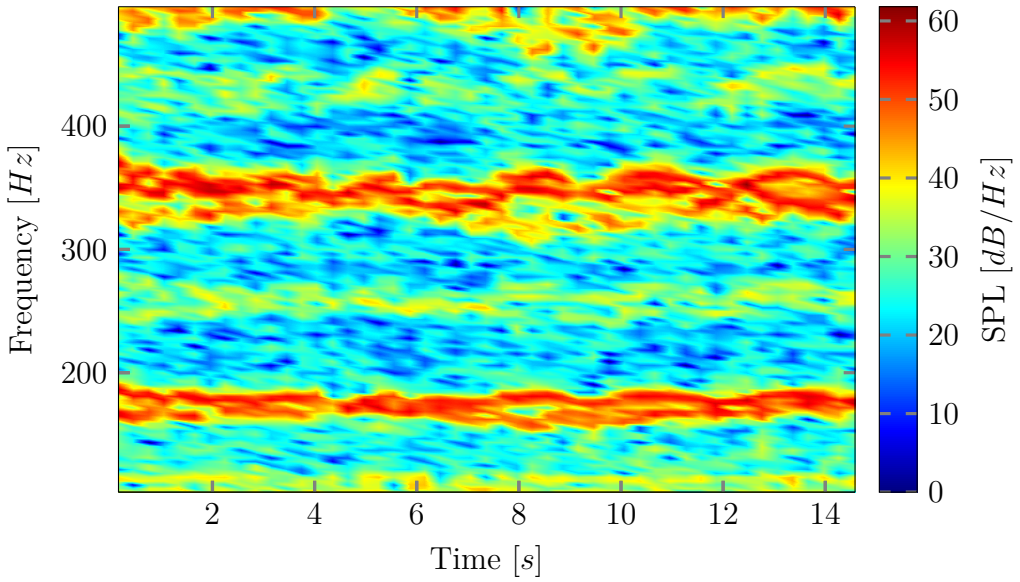

FIGURE 4.8: Spectrogram of the drone noise in hover inside JAFAAR recorded by microphone 1

Also by comparing the results obtained with this spectrogram and the ones in Figure 4.6, this last has its four propellers rotating at the same speed because the BPF of each rotor is the same. This observation supports the fact of making the measurements outdoors.

4.2 Maneuvers analysis

The purpose of this thesis is to analyze the sound produced by a drone during its different maneuvers and associate it with noise annoyance/psychoacoustics. For that, the noise is analyzed with the RMS graph, power spectrum and spectrogram.

Hover

The first and simplest maneuver is the hovering phase. As explained in Section 3.5, it consists of a stationary flight between the four microphones. As the drone is flown manually by means of a controller, its position is not totally constant along time. In fact, because of the wind and the self stabilizer, the drone could move closer to a microphone than another.

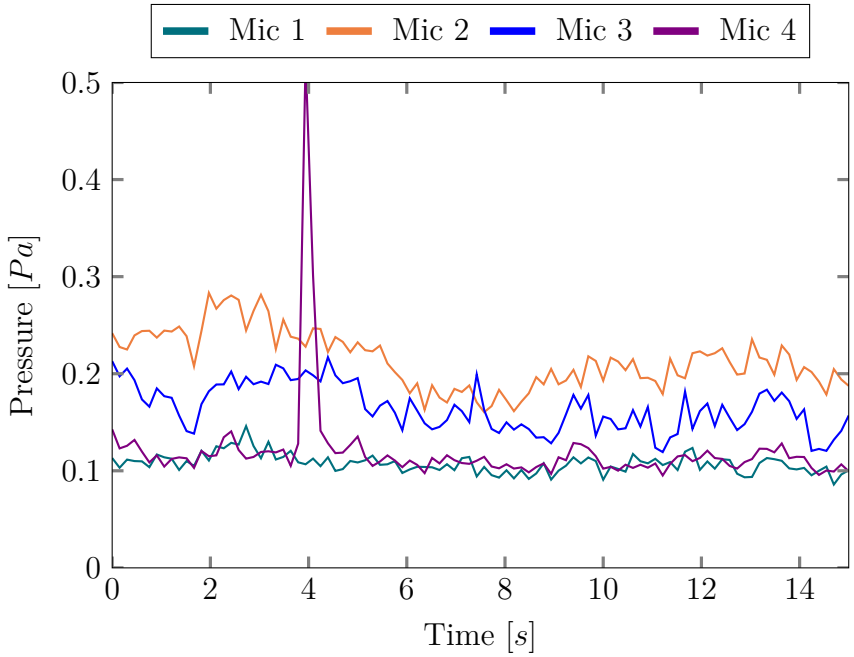

FIGURE 4.9: Root mean square graph of the hovering outdoors recorded with the 4 microphones

Firstly, Figure 4.9 shows that there was an error for microphone number 4 at 4 seconds. Then, it shows that the drone was flying closer to microphones 2 and 3 and particularly to the second one. Otherwise, the noise produced by the drone in a hovering flight remains constant along time.

The spectrum of the drone in hovering flight (Figure 4.10) shows the frequencies and their intensity produced by the drone during 15 seconds. It can be seen that the first peak represent the blade passing frequency (BPF) and the other one are their harmonics. This BPF appears at 170 Hz which correspond to 5100 RPM for the propellers. This calculation is explained in Equation (2.1). Also, as already explained in Section 2.4, the two peaks

appearing at 3500 and 5500 Hz are coming from the electric motor and these peaks appear in each maneuver.

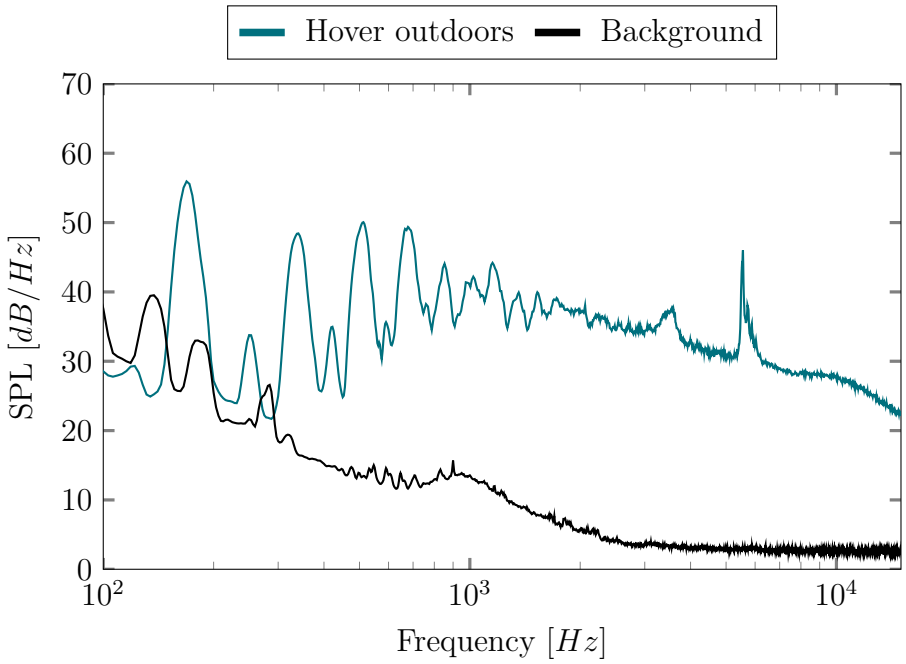

FIGURE 4.10: Spectra of the hovering maneuver outdoors. BPF = 170 Hz

The spectrum obtained is comparable to the one obtained also outdoors by Alexander and Whelchel [8]. The main BPF and its harmonics are well defined in the lower frequencies (below 1kHz). Then, research conducted by Zawodny *et al.* [33] was performed in an anechoic chamber with a fixed drone. The spectra show clear BPF and Harmonics till 2000 Hz due to the absence of background noise. Finally, the results obtained numerically by Afari [34] for one propeller shows the same behavior. However, the UAVs used in these researches was not the same as for this thesis. This difference leads to not exactly the same BPF and intensities.

In Figure 4.11, the spectrogram for the hovering flight in the range from 100 to 15,000 Hz is plotted.

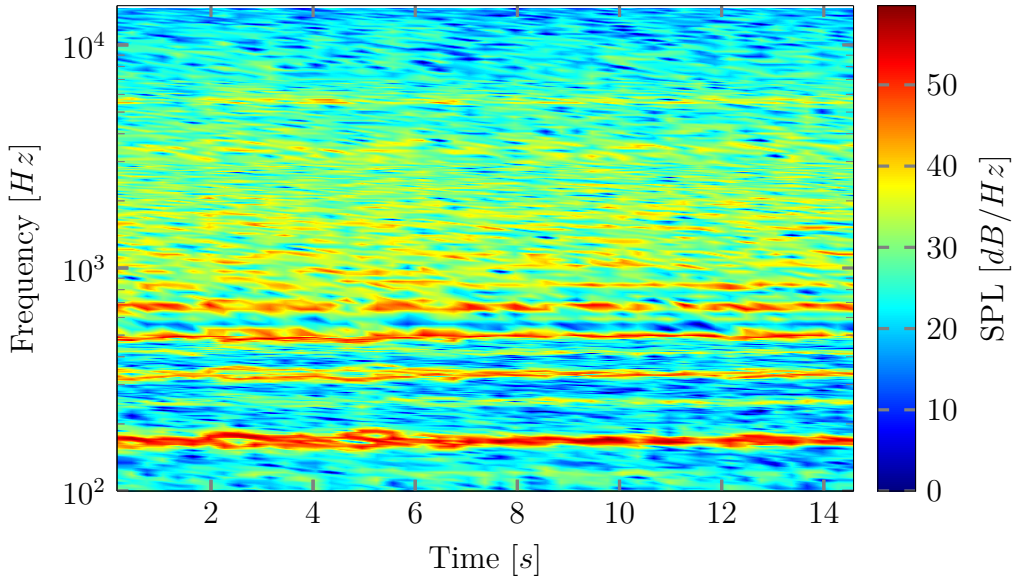

FIGURE 4.11: Whole spectrogram of the drone noise in hovering flight recorded by microphone 1

In this Figure, the first BPF can be seen at 170 Hz and the other lines in red are the harmonics. Over 1000 Hz as can be seen in the spectra, the noise is dominated by broadband. However, the last peak coming from the electric motor is seen between 5000 and 6000 Hz. However, as the interesting low frequencies are difficult to analyze, the next spectrograms for all maneuvers will be in a range from 100 to 500 Hz. The one for the hover is shown in Figure 4.12.

The spectrogram including all the frequencies has the same shape as the one obtained by Alexander and Whelchel [8]. The main BPF and its harmonics are visible thanks to their higher intensities in the spectrum. The frequencies and intensities obtained are not the same given that the drone used for this research is not a DJI Phantom 3 SE.

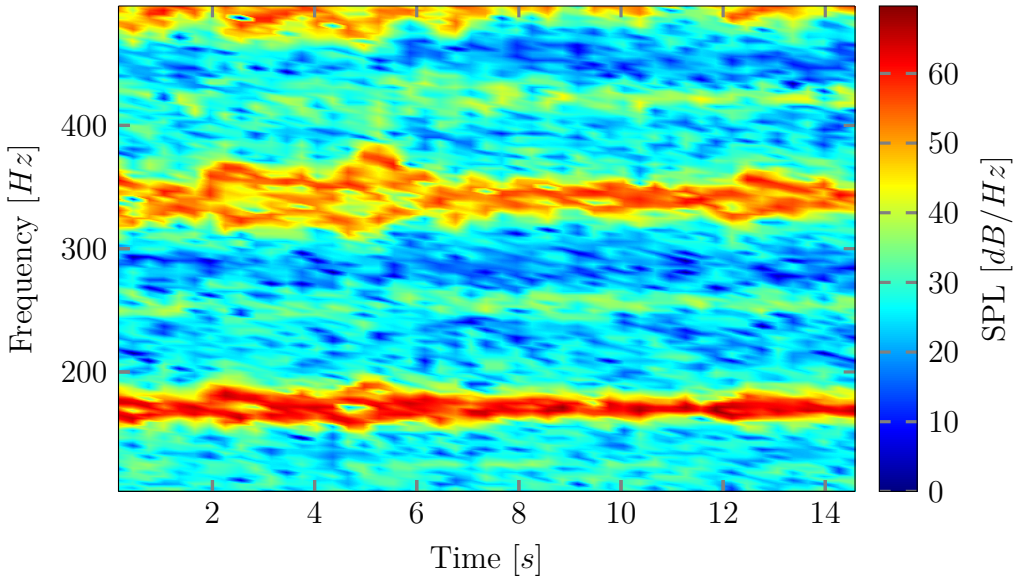

FIGURE 4.12: Spectrogram of the drone noise in hovering flight recorded by microphone 1

In Figure 4.12, the main BPF can be easily found at 170 Hz. As already explained in Section 4.1, the frequency line of the BPF is not totally straight because of the changing rotational speeds of the propellers. In fact, the drone wants to stabilize itself and stay in the same position. Therefore during a short time, one or several propellers need to change their speed and it induces some splitting lines for the BPF and its harmonics. Otherwise, it can be seen that the drone stays mostly steady and the frequencies do not vary a lot.

Fly-over

The second maneuver analyzed is called the "fly-over". It is explained in Section 3.5 and schematized in Figure 3.9.

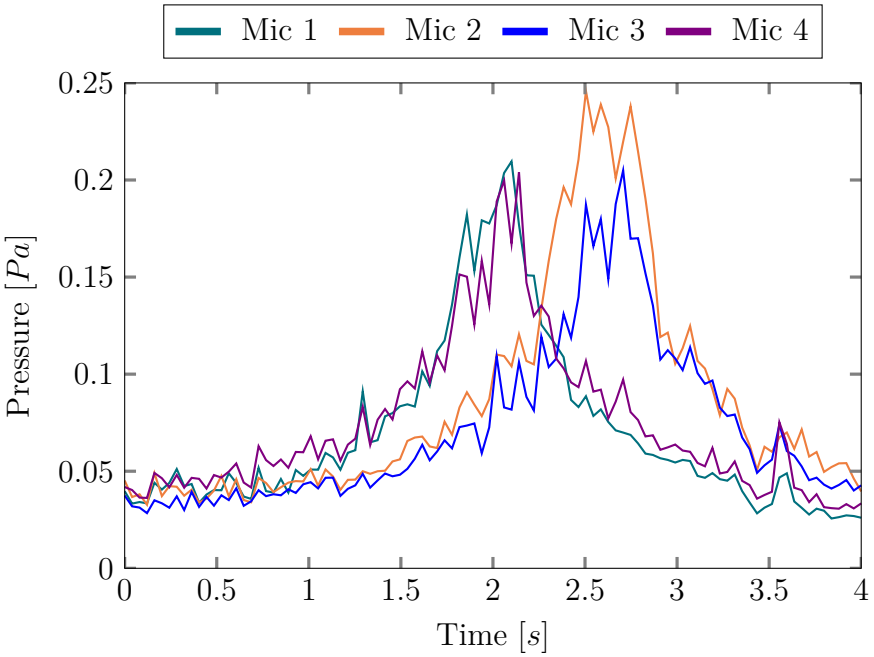

FIGURE 4.13: Root mean square graph of the drone passing over the 4 microphones

Figure 4.13 shows the RMS of the pressure recorded by the 4 microphones of the drone passing by over these ones. As it can be seen in the scheme Figure 3.9, the drone passes closer to microphones 1 and 4 first and then closer to the 2nd and 3rd ones.

To compare the pressure measured with the hovering flight, it can be seen that the maximum values of the fly-over are not particularly higher.

The spectra of the fly-over (Figure 4.14) shows different behavior. Firstly, the peaks are not well defined. In this configuration, the front propellers have not the same rotation speed as the rear ones, which means that the tonal peaks expand over a larger frequency range. The BPF are thus not the same for the front and the rear rotors. Otherwise, the intensity of the BPF and its harmonics are quite comparable to the hover flight noise.

The spectrum obtained for the fly-over in the research of Alexander and Whelchel [8] shows that in low frequencies, the number of separate tones increases because of the varying

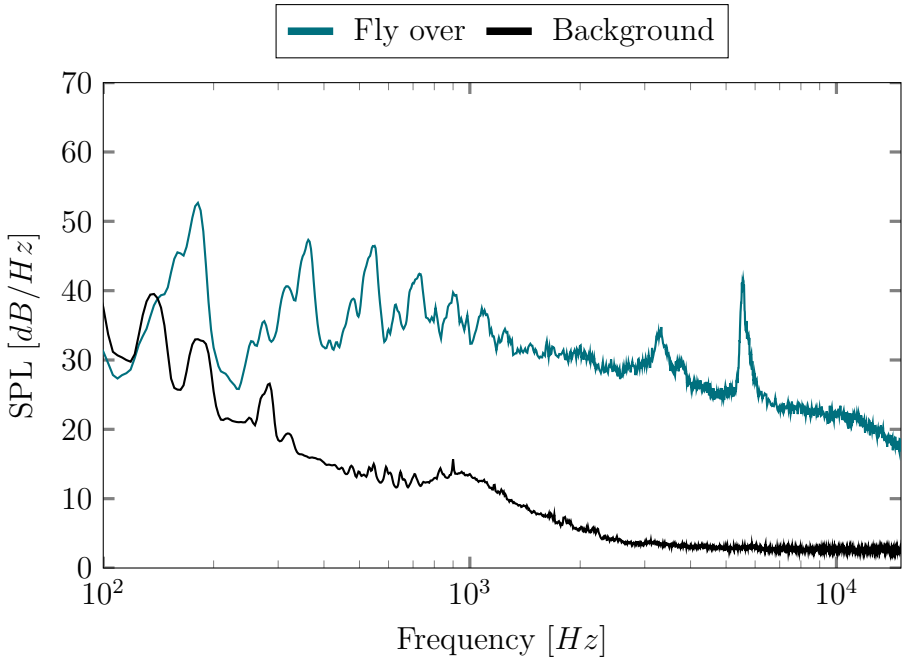

FIGURE 4.14: Spectra of the drone passing over the microphones. BPF = 179 Hz

rotational speeds of the propellers in forward flight. In other words, the BPF and harmonics peaks are thicker in this configuration than the one obtained in hovering flight. This separated tones has been clearly shown by Zawodny *et al.* [33]. With their fixed drone in an anechoic wind tunnel, the tones obtained for the front and rear propellers in forward flight are distinctly discerned.

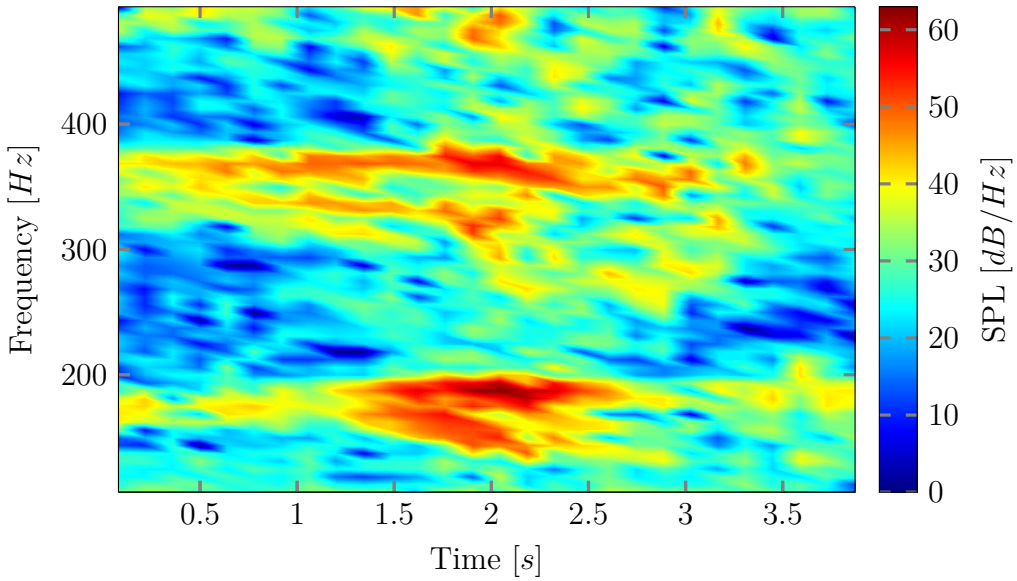

FIGURE 4.15: Spectrogram of the drone noise in fly-over recorded by microphone 1

Figure 4.15 shows the spectrogram of the fly-over. At the moment when the drone is passing over the microphone at two seconds, it can be seen that the BPF is not a single line but a splitting one. Such as the transition phase. It means that the rotors are rotating

at different rpm when the drone is flying forward.

Transition

The transient phase, called in this thesis "transition" maneuver, is described in Figures 3.11 and 3.12. This maneuver is important to analyze and to compare with the others. From a psychoacoustic point of view, the human ear is mostly more annoyed when there is a variation of the frequencies and of intensity (Loudness) in time [35]. And the transition maneuver experiences these two variations.
The recording of the transition maneuver and their 4 phases (Figure 3.12) took only 5 seconds. During this time, the drone is coming, decelerating, hovering and finally going forward again.

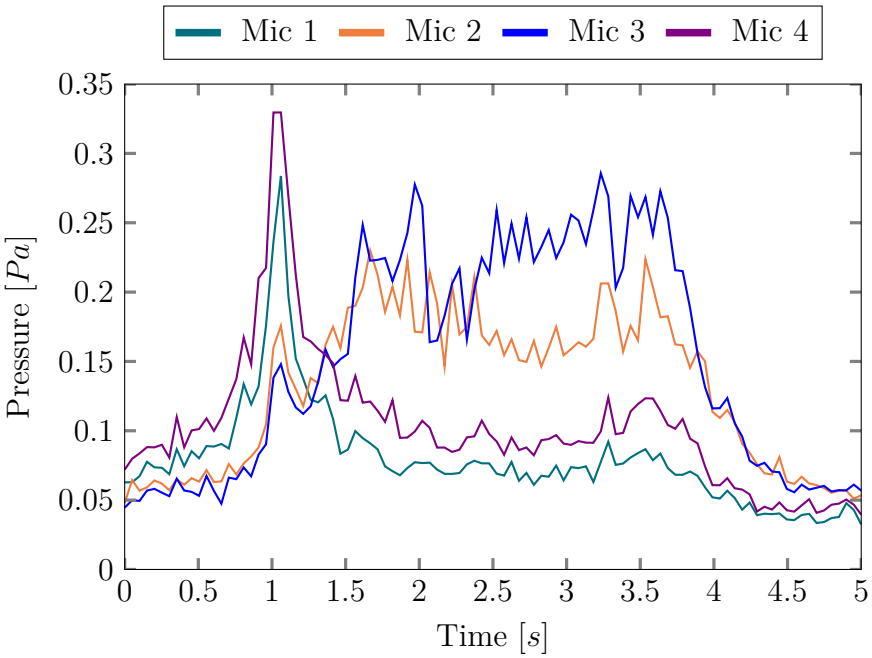

FIGURE 4.16: Root mean square graph of the drone decelerating, stopping and going forward between the microphones

Figure 4.16 shows the RMS graph of the transient maneuver. With this graph, the different phases of this maneuver (schematized in Figure 3.12) can be determined. The drone was flying forward to the microphones' square and began to decelerate at 1 second. Then at 1.5 seconds, it can be seen that microphones 2 and 3 are recording higher noise, it is still due to the position of the drone, closer to these ones and not precisely on the square center. Finally, the drone was accelerating at 3.5 seconds where an increase in pressure can be detected. What mainly emerges is that the RMS are constant in time during the hovering flight, while the decelerating phase at 1 second is characterized by an increase in pressure leading to a higher level of noise.

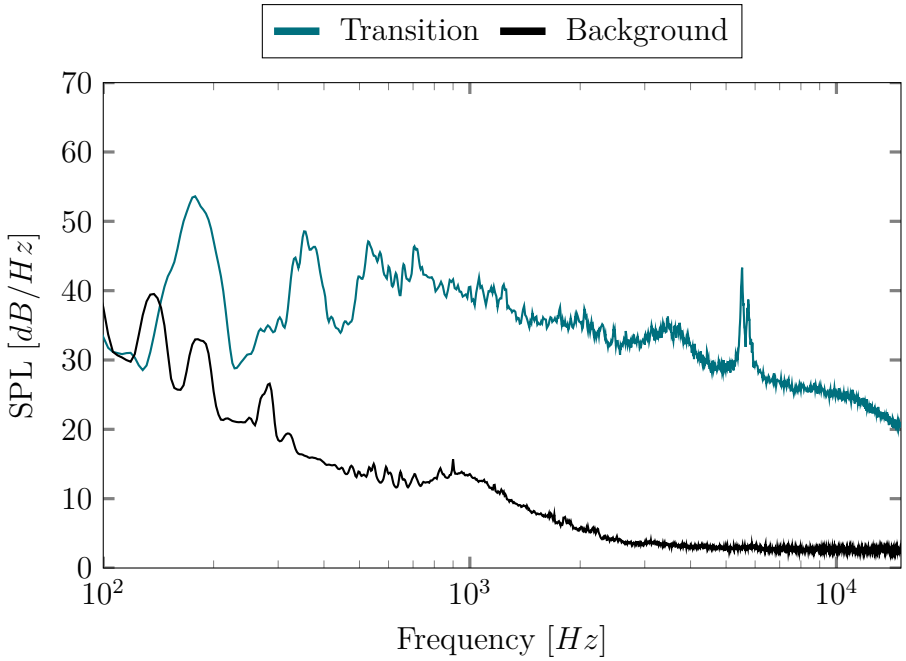

FIGURE 4.17: Spectra of the transient maneuver between the microphones. BPF = 180 Hz

Figure 4.17 shows the spectrum of the 5 seconds transition phase of the drone. Like the fly-over maneuver, the BPF peak is broader. It shows that the range of frequencies is wider. This is due to the transition maneuver, the front and rear propellers have not the same rotation speed. Therefore the broadband noise is dominant and there are no well defined small peaks like in Figure 4.10 in hovering flight. The noise produced by the electric motor between 5000 and 6000 Hz is represented by two peaks instead of one in the steady flight (Figure 4.10). In fact, the variation of rotational speed to decelerate or accelerate are due to a change of power of the electric motors and therefore, their tone.

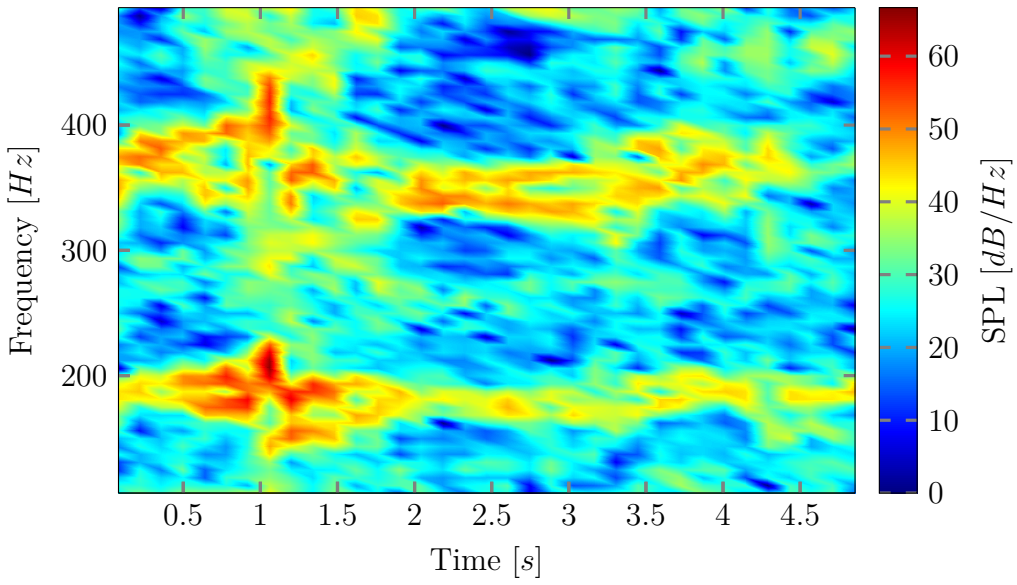

FIGURE 4.18: Spectrogram of the drone noise in transition recorded by microphone 1

Figure 4.18 shows the spectrogram of the transition maneuver. The evolution of the graph is interesting because the different phases are well defined. Starting from 1 second, it corresponds to the decelerating phase. A splitting frequency can be observed at this time. Therefore the splitting frequency means that the rotation speeds of the front rotors are not the same as the rear ones with the link of the BPF in Equation (2.1). It can be deduced, with the stability of the drone, that the front ones have a higher rpm. After the decelerating phase occurs the hovering phase, like in Figure 4.12, where the BPF matches and are the same. Finally, the accelerating phase induces a smaller splitting frequency but is still present.

Tilting

The called "tilting" maneuver, explained and schematized in Figure 3.10, has been recorded in order to obtain a long record of the transient phase. During all the measurements, the drone was accelerating and decelerating. With a long record, it permits obtaining more accurate results for the spectrum.

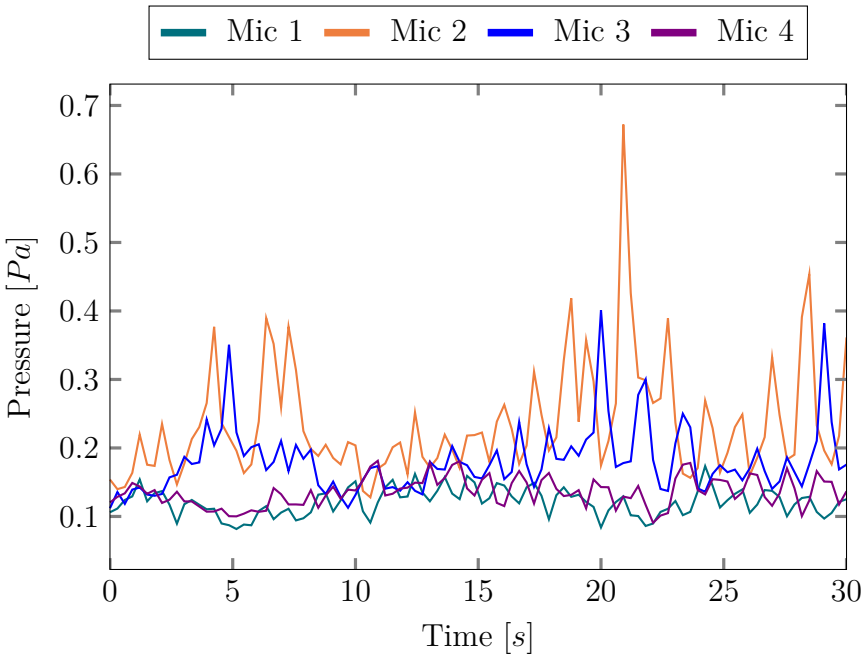

FIGURE 4.19: Root mean square graph of the drone making back and forth between the mic 1-2 and mic 3-4

By looking at the RMS graph of the tilting maneuver (Figure 4.19), it can be seen that the drone was flying closer to microphones 2 and 3. By checking these results and comparing them with the ones obtained in hover, some peaks in the transition record give higher pressure. In general, for these two microphones, the pressure is higher than the one obtained for the hovering flight in Figure 4.9. At 21 seconds approximately, the peak can be associated with the presence of the drone flying over the microphone 2, hence it can be

interpreted as a wake distortion effect. Moreover between 4 and 7 seconds, and between 19 and 24 seconds, as the drone is flying back and forth rapidly, the peak is shifted among two microphones in a range of time corresponding to the one that the drone takes to change its direction.

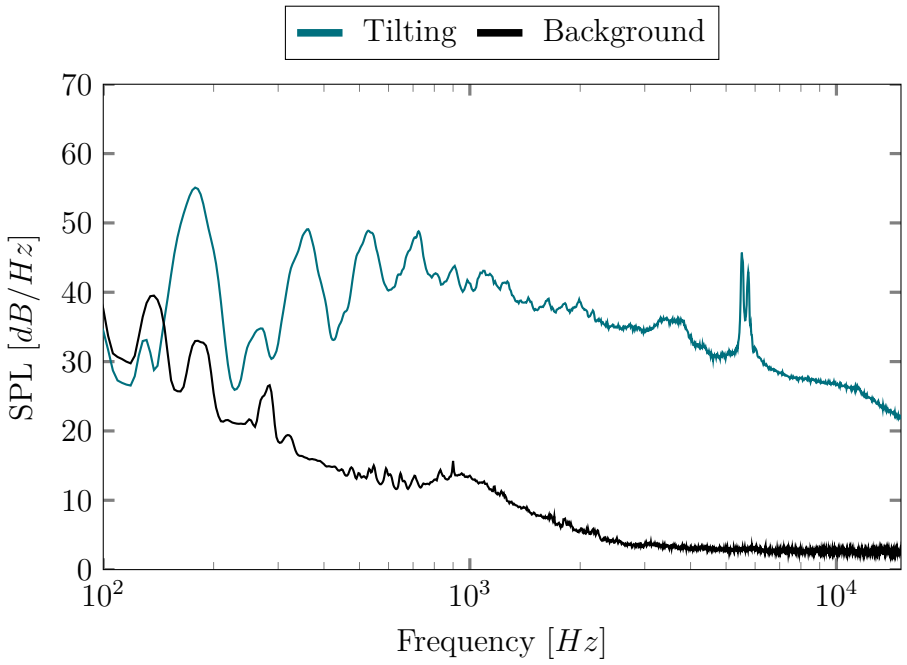

FIGURE 4.20: Spectra of the drone flying back and forth between mic 1-2 and mic 3-4. BPF = 178 Hz

Figure 4.20 shows the spectrum of the tilting maneuver recorded during 30 seconds. With this long-time record, it is easier to obtain more accurate results about the frequencies present during the transient maneuver of the drone (Figures 3.11 and 3.12). During this maneuver and as explained just above, a larger range of frequencies for the BPF and its harmonics are present in the noise. In fact, because of the changes of direction, inclinations, accelerations and slowdowns, the propellers were changing their rotational speed. Therefore, the change of RPM induces a change of BPF. The same observation as in the transient maneuver about the tone of the electric motor can be made. The accelerating and decelerating phases of the drone induce a variation of the electric motor power and so, its tone. The peak of the electric motor is then split in two for the rear and front motors. However, the mean BPF computed and found in the spectra are relatively the same. The change of rotation speed of the propellers happens during a very short time. The spectrograms are used to check these variations such as in Figures 4.12, 4.15 and 4.18.
The last spectrogram shown in Figure 4.21 shows the evolution of the frequencies along time for the tilting maneuver.
This figure demonstrates that the drone was flying back and forth all the time. These changes of direction induced a difference in rotational speed for the different propellers, as can be seen for the transition maneuver.

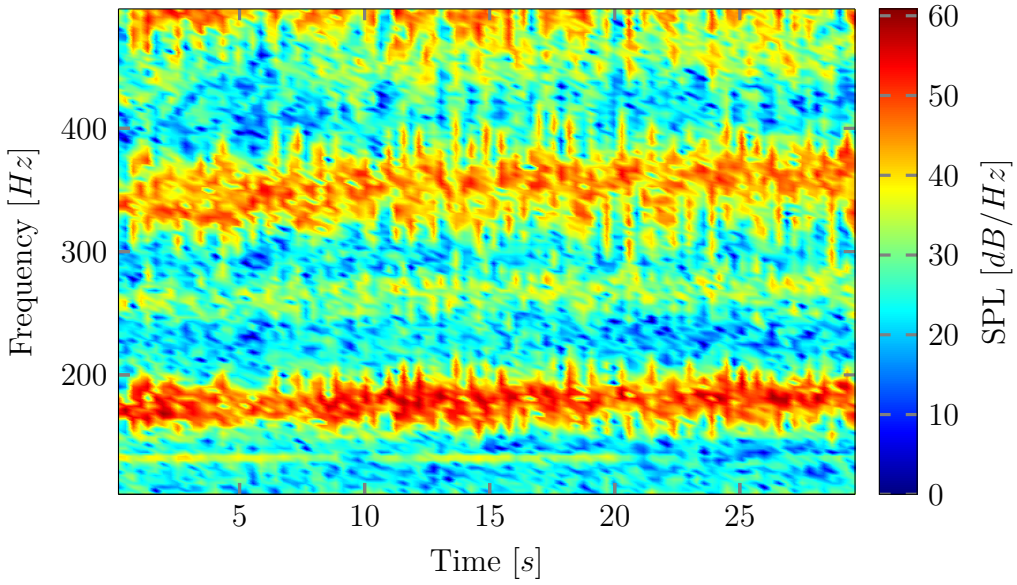

FIGURE 4.21: Spectrogram of the drone noise in tilting recorded by the microphone 1

4.3 Psychoacoustics analysis

In this section, three different metrics used in psychoacoustics and noise quality analysis will be used to characterize the different maneuvers of the drone. The metrics are defined and explained in Section 2.3. The analysis has been performed for two microphones only: mic 1 and mic 3. As can be seen in Figure 3.2, the selected microphones are opposite to each other. By comparing them, a link between the directivity and the noise annoyance is performed.

Loudness

Figures 4.22, 4.23, 4.24 and 4.25 show the loudness of the hovering flight, fly-over, tilting and the transient phase respectively.

For all loudness graphs, a relation between them and the RMS graph for each maneuver can be observed. When the pressure on the microphone increases significantly, the loudness follows it. The different intensities of the loudness can be discussed. The hovering flight (Figure 4.22) has a quite constant loudness and there is no specific change between the two microphones. The loudness stands around 60 sone. This value appears also when the drone is hovering during the transition phase (Figure 4.25) for mic 3. In fact, as can be seen also in the RMS graph Figure 4.16, the drone was closer to mic 3 than mic 1 and therefore the intensity decreases for this last one. In this same loudness figure, a peak can be observed after 1 second at 80 sone when the drone is decelerating and flying over mic 1. Even if the intensity by passing over the microphone increases, it does not vary the increase of loudness for the microphone 3. The loudness increases because the drone is approaching till 2 seconds when it begins to hover. Finally, a small increase is observed when the drone

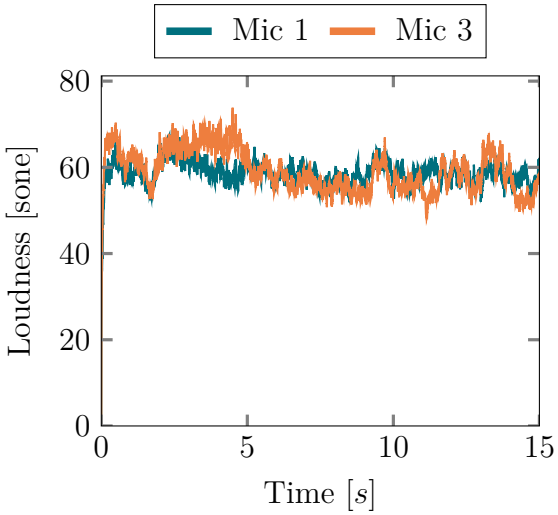

FIGURE 4.22: Loudness in hover for microphone 1 and 3

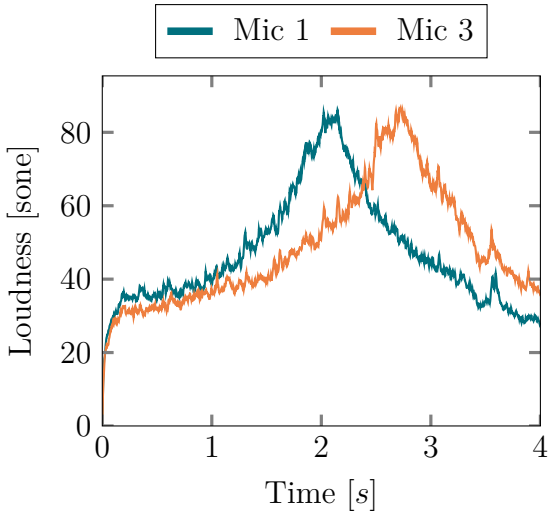

FIGURE 4.23: Loudness in fly-over for microphone 1 and 3

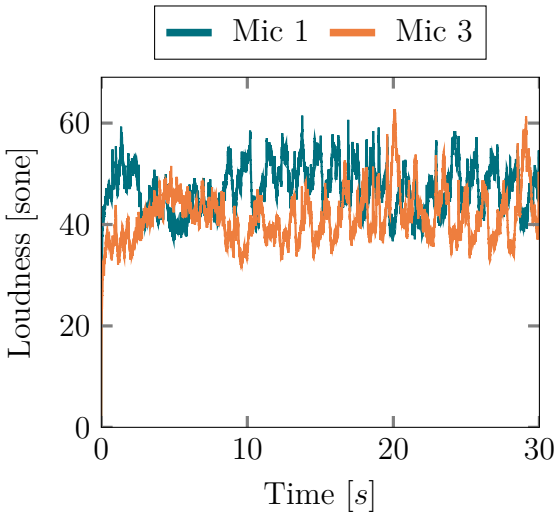

FIGURE 4.24: Loudness in tilting for microphone 1 and 3

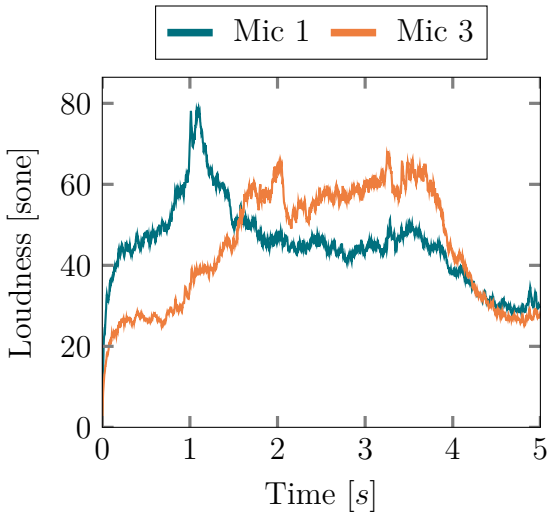

FIGURE 4.25: Loudness in transition the microphone 1 and 3

accelerates between 3 and 4 seconds. The approaching phase loudness can be analyzed with the fly-over loudness graph in Figure 4.23. Loudness for both microphones seems the same with a shift. This shift is due to a maximal value when the drone is passing the closest to the respective microphone. This shape can be compared to the RMS graph in Figure 4.13. However, the peak at around 80 sone is comparable to the one of the deceleration observed in Figure 4.25. It involves that there is no difference in loudness when the drone is flying at a constant speed and when it is decelerating. Finally, Figure 4.24 represents the loudness of the tilting maneuver. It can be seen that the loudness varies a lot with time as the drone is doing back and forth between the microphones as explained in Section 3.5. But also that the intensity is lower than the other maneuvers as hovering and flying-over. The values of the loudness in hover obtained in the research of Torija *et al.* [36] is lower and stands around 27 sone. The one measured by Besnea [37] is also lower ($\approx$ 20 sone).

In these two papers, they use different software to compute it. Torija computes it with ArtemiS from Head Acoustics [38] and Besnea used LabView [28] although MoSQUITo [13] is employed for this thesis.

Sharpness

The second psychoacoustic metric is the sharpness, defined in Section 2.3. It is represented in Figures 4.26, 4.27, 4.28 and 4.29 for the hovering flight, the fly-over, the titling and the transition phase respectively.

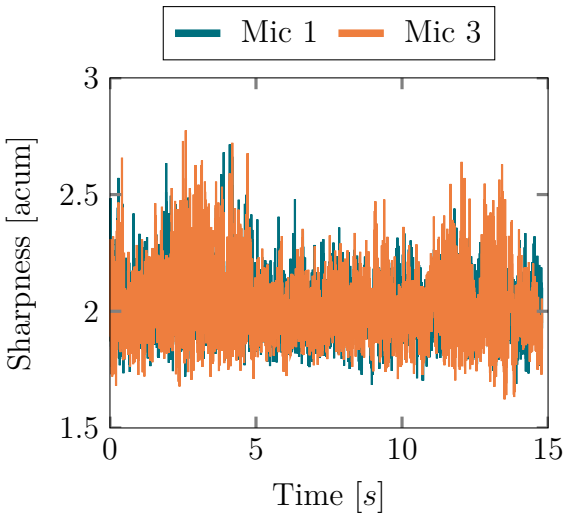

FIGURE 4.26: Sharpness in hover for microphone 1 and 3

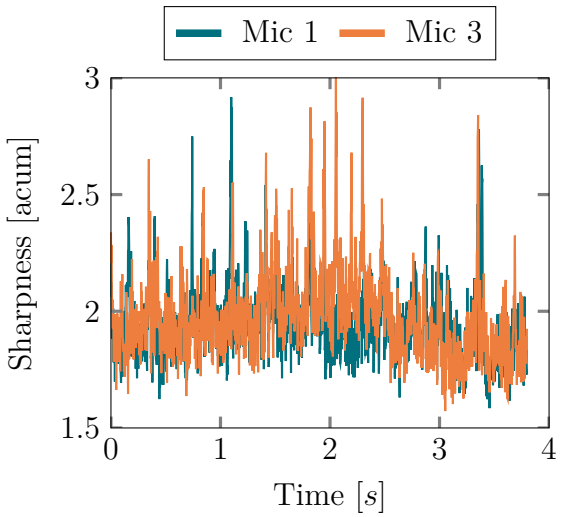

FIGURE 4.27: Sharpness in fly-over for microphone 1 and 3

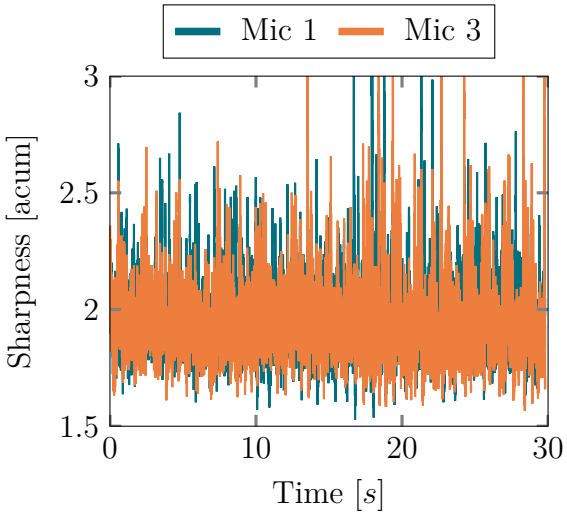

FIGURE 4.28: Sharpness in tilting for microphone 1 and 3

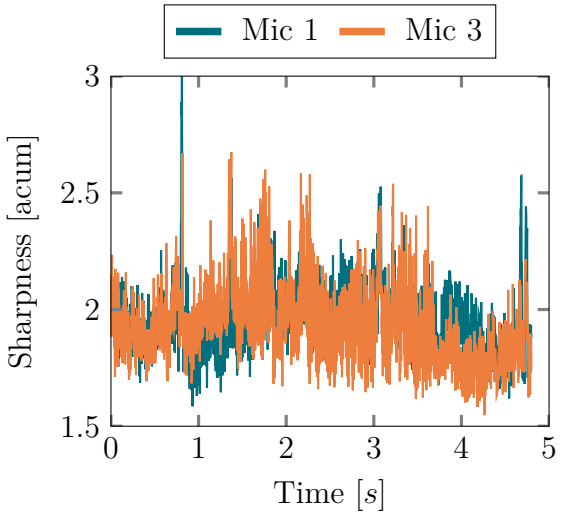

FIGURE 4.29: Sharpness in transition for microphone 1 and 3

As it can be seen in each graph, the mean value of the sharpness stand around 2 acum. However, some peaks are present in Figure 4.27 when the drone is passing over the microphones at around 2 seconds. The sharper the sound, the more "bee-like" the sound is.

In hovering flight, the peaks are rarely crossing 2.4 acum. When it is the case, it means that there was a change in rpm of the propellers (as shown in the spectrogram figure 4.12) between 2 and 5 seconds. Some significant peaks are also occurring in the tilting maneuver, when the drone is going back and forth between the microphones, in Figure 4.28. The drone is constantly changing its angle of attack which induces more wake interaction. This apparently leads to variation in sharpness.

Besnea [37] obtained approximately the same results in her research. However, Torija *et al.* acquired higher values for the sharpness (around 3.5 acum) for the hovering flight.

Roughness

The last metric analyzed is roughness. It depends on the modulation of the sound, as explained in Section 2.3. The graphs are represented in Figures 4.30, 4.31, 4.32 and 4.33 for the hovering flight, the fly-over, the tilting and the transition phase respectively.

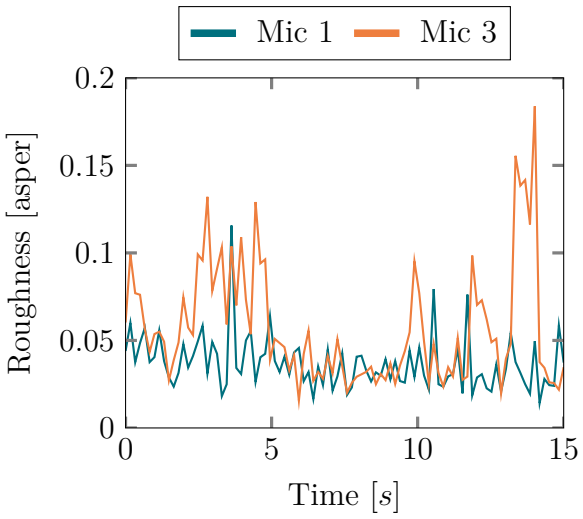

FIGURE 4.30: Roughness in hover for microphone 1 and 3

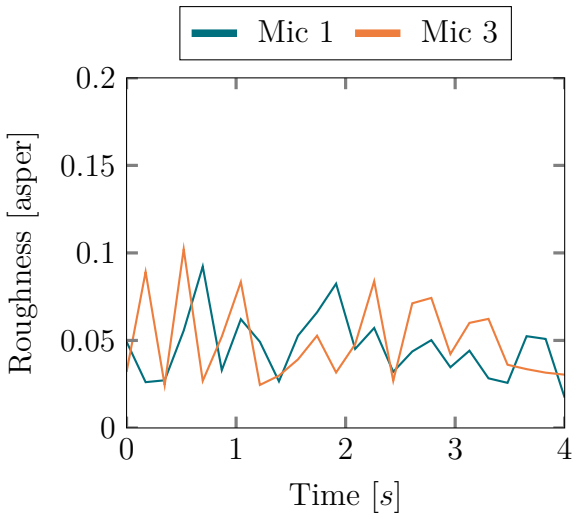

FIGURE 4.31: Roughness in fly-over for microphone 1 and 3

The difference of points in the fly-over and transition graphs in Figures 4.31 and 4.33 are due to the code and the window that MoSQUITo takes to compute the roughness. However, some peaks can be perceived over 0.1 asper in the tilting maneuver in Figure 4.32 as well as for the hovering flight in Figure 4.30 and the hovering phase in Figure 4.33.

As it can be noticed, the results obtained for the roughness with the software MoSQUITo give lower values than the ones obtained in the thesis of I.Besnea [37] obtained with LabView (around 0.3 to 0.6 asper). The computation of the roughness obtained with ArtemiS by Torija *et al.* is really higher and stands around 2.1 asper. As mentioned in Section 2.3, no normalization on the computation of the roughness has been done yet. The difference between the several software can come from this lack of information about this metric.

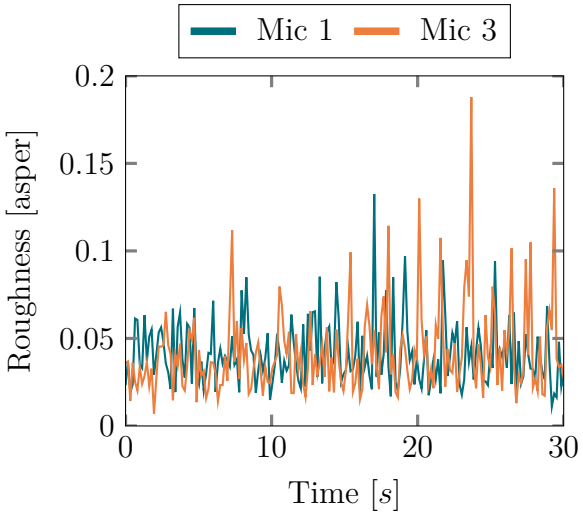

FIGURE 4.32: Roughness in tilting for microphone 1 and 3

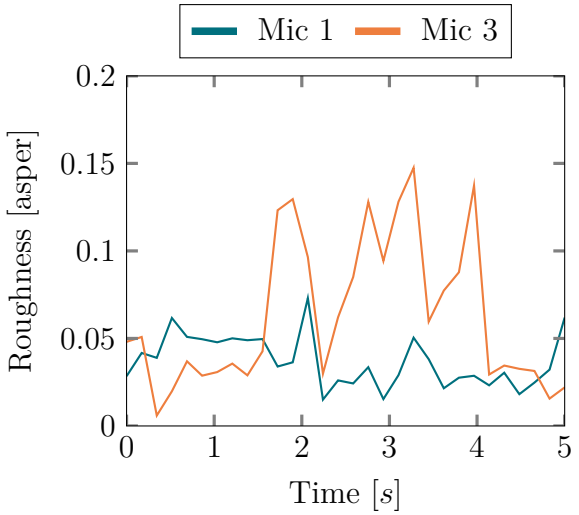

FIGURE 4.33: Roughness in transition for microphone 1 and 3

4.4 Flight noise analysis

This section interprets the different results and graphs obtained for each maneuvers in the precedent sections. First, the BPF and the RPM are compared to understand the behavior of the drone. Then the psychoacoustic and noise annoyance are discussed to define the most annoying maneuvers.

Main BPF and RPM

As it can be seen in the different spectra for each maneuver, the Blade-Passing Frequencies are not exactly the same. These ones are gathered in Table 4.1.

	Hover	Fly-over	Transition	Tilting
BPF [Hz]	170	179	180	178
RPM	5100	5370	5400	5340

TABLE 4.1: Blade-Passing Frequency (found with the methodology explained in Section 4.1) and rotational speed (computed with (2.1)) of each maneuver.

By looking at this table, it appears that the hovering flight has a smaller BPF than the moving maneuvers. This observation is trivial because these three last maneuvers lead to having a pitch angle. And because of this angle, the drone needs more vertical lift to stay at the same altitude and therefore the rotational speed increases as well. However, this table and the graphs give the BPF of the drone and not the BPF of each propeller. It can be seen by the thicker main peak in the spectra (in Figures 4.14, 4.17, 4.20) that it covers a bigger range of frequencies. As already said, it is because the front and rear propellers are not rotating at the same speed.

Maneuvers noise interpretations

The hovering flight, fly-over and the transition phase are three common maneuvers during a drone flight. Therefore, these three are compared to determine which is the most annoying for the human ear. Therefore, the spectra, the spectrogram and the psychoacoustics metrics present in Sections 4.2 and 4.3 will be used.

First of all by focusing on the spectrograms, the three maneuvers are different. For the hover (in Figure 4.12), the BPF and its harmonics remain reasonably constant along time. There is no consequent change of rotational speed for either propeller. The frequencies involved in the noise as well as their intensity are constant with time. However, for the fly-over (in Figure 4.15), it can be seen that a wider range of frequencies is taken when the drone is flying over between 1 and 3 seconds. Even so, there is no dramatic change in frequencies. As explained in the previous Section 4.2, when the drone is flying forward, the front propellers are not rotating at the same speed as the rear ones. This induces this wide range in frequencies. Finally, for the transition phase (shown in Figure 4.18), it can be seen that there are splitting lines between 0 and 1 second and between 1 and 2 seconds, the lines are merging. As already explained, this is due to the decelerating phase of this maneuver where the front and rear propellers are not rotating at the same speed. The variation of the intensity and the frequencies along time causes a more annoying noise [35].

Then by checking the spectra for the frequencies present in the noise, one can notice that the fly-over and the transition cover more frequencies in the main BPF peak (Figures 4.14 and 4.17 respectively) compared to the hovering flight (Figure 4.10). However, no link between noise annoyance and a bigger range of frequency has been done.

The next comparison of these maneuvers is focusing on the psychoacoustic metrics. Firstly regarding the roughness, one can see that there is no difference between the three maneuvers (shown in Figures 4.30, 4.31 and 4.33). Some peaks can happen but are not significant enough. As already said in Section 4.3, the roughness computation is confused.
The next metric to compare is the loudness. The hovering flight shows a constant loudness of 60 sone (Figure 4.22) while when the drone is flying over the microphones (Figure 4.23) and when the drone is decelerating over the mic 1 (Figure 4.25), the loudness reaches a peak of approximately 80 sone. It means that when the propellers do not rotate at the same speed, the loudness is increased. Also, the mean RPM is higher for the maneuvers comparing the the hover (shown in Table 4.1).
The last psychoacoustic metric to compare is the sharpness. This last stays approximately around the same value, 2 acum, for each maneuver. However, some peaks can be observed

when the drone is flying over the microphones, at 2 seconds, in Figure 4.27. The sharpness can reach 3 acum. Some peaks can be noticed in Figure 4.29 between 1 and 2 seconds when the drone is decelerating during the transition. Finally, some increase of sharpness can be perceived in Figure 4.26 when the drone is hovering between 2 and 5 seconds. During this time, as can be seen on the spectrogram Figure 4.12, the propellers are not rotating at the same speed. Therefore, a relation could be made by linking the increase of sharpness if the propellers are not rotating at the same speed.

For quantifying annoyance, a jury panel of individuals subjected to a range of sounds rank the annoyance of these samples. Statistical analysis permit to find some empirical correlations between the SQM and the reported annoyance. Obviously, there is a large variability between the individuals related to their history, cognitive biases, etc. This equation is therefore a first approximation. The Psychoacoustic Annoyance (PA) can be expressed for the overall annoyance response to a certain sound. An empirical model taking into account the sound quality metrics have been developed by Zwicker [16] and is shown in Equation (4.1).

$$PA^{1} \approx N_5 \left(1 + \sqrt{w_S^2 + w_R^2}\right) \tag{4.1}$$

with

- N_5 percentile loudness exceeded 5% of the time in sone
- $w_S = (S - 1.75) \cdot \log_{10}(N_5 + 10)$ for $S > 1.75$. The sharpness S is in acum.
- $w_R = \frac{2.18}{N_5^{0.4}}(0.6R)$. The roughness R is in asper.

It can be seen that the loudness and sharpness have a bigger weight on the annoyance compared to the roughness as the loudness is high.

This equation will give an approximation of the psychoacoustic annoyance. Other sound quality metrics exist and can be added in this equation to give a better approximation. These results compared to the ones obtained in the research of Torija *et al.* [2] are in the same order of magnitude but a bit lower with Equation 4.1 ($\approx$ 45 to 75 in hover with a DJI Phantom 3 at 1 or 2m above the ground and between 0 to 5m next to the microphone). Besnea [37] has got lower values for the PA in each maneuver of a sUAV (DJI Phantom 4), below 40. These results come principally from the value of the loudness obtained in Section 4.3 which is twice the value that the one obtained by these researchers.

Also, the annoyance for the human ear explained with the help of the spectrograms and [35] is not taken into account in the computation of the PA score.

[1] The formulation of this expression is modified because of the absence of the fluctuation strength

All these differences are gathered in Table 4.2 to compare the three maneuvers noise annoyance.

	Hover	Fly-over	Transition
Frequency range thickness	-	+	+
Frequency variation with time	-	-	++
Roughness	/	/	/
Loudness	+	++	++
Sharpness	+	++	++
Psychoacoustic Annoyance (PA)	87.7	158.2	144.2

TABLE 4.2: Comparison of the annoying sources for the hover, fly-over and transition maneuvers. Legend: '-': No significant; '+': Significant; '++': Very significant; '/': Not relevant

With this table and this discussion, it appears that the fly-over and the transition maneuvers are more annoying to the human ear than the hovering flight.

5 Conclusions

The objective of this research was to compare the drone noise in its different flight maneuvers. Throughout this study, different analysis have been performed in order to determine the noise annoyance of these maneuvers. This thesis is a preamble of future studies related to drone noise and noise annoyance, in a world where the use of small UAVs is continuously increasing. The understanding of drone noise is fundamental with the inevitable new infrastructures and all sizes UAVs in the coming years.

To achieve this first approach of drone noise, the sUAV DJI Phantom 3 SE has been used. The drone flew by performing different maneuvers that are common for a quadrotor UAV such as the hover, the fly-over and the transient phase. The power spectral densities and spectrograms have been investigated for each maneuver. These first permitted to reveal the frequency ranges of interest and the Blade-Passing Frequencies. Lastly, some sound quality metrics were computed for each maneuver to obtain a first evaluation of the noise annoyance.

Some sound assessments have been firstly performed to check if the recorded sound can be analyzed. As the research question is to study the different drone maneuvers noise, the comparison between the measurements taken in an anechoic chamber and outdoors have been performed. The sound recorded inside the chamber is atmospheric noise-free. A second analysis was to measure the sound at different altitudes to check if the drone is flying without interaction with the ground.

The spectral analysis showed in all cases that the Blade-Passing Frequencies and harmonics were dominant in the low frequencies. The broadband noise hindered the tonal one above 2000 Hz. Thanks to this analysis, the mean BPFs have been computed. A difference between the hovering flight and the moving maneuvers could be found due to the pitch angle of the drone. In fact, with a certain angle, the drone needs more vertical lift to keep the same altitude and the rotational speed of the propellers needs thus to be increased.

Then the spectrograms permitted to show the frequencies involved with time of each maneuver. For the hovering flight, the four propellers were rotating at the same rotational speed while for the other three maneuvers, the propellers were varying their speed.

Finally, the sound quality metrics have also been calculated per maneuver. With these lasts, the possibility to find the most annoying maneuver is that the transition phase as well as the fly-over are more annoying compared to the hovering flight.

During this research, some constraints have been encountered. As already explained in the thesis, the drone was flown manually with the help of a controller. Also, the drone was able to stabilize itself. Therefore with the weak wind, the drone was not completely steady in the center of the microphones' square for the hovering flight. It induced different values of the pressure and the noise between the microphones although they should obtain approximately the same value.

Another constraint stands in the anechoic chamber measurement. Because of the small space where the drone was flying, some wake induced a difference in the rotor speed and only the hovering flight was possible.

5.1 Conclusions

Thanks to the summary of the thesis, the different research questions can be answered. Firstly, the measurements carried out outdoors permits to analyze the different sources of noise since the frequency of this source remains below 2000 Hz.

Secondly, the RMS graph, the spectral analysis and the spectrograms permit to find differences in the noise produced in the different flight configurations. Also, the behavior of the drone and its propellers can be deduced thanks to these graphs.

The last topic focused on noise annoyance. It has been concluded, with the help of the spectrograms and Sound Quality Metrics, that the moving maneuvers as the fly-over and the transition are more annoying for the human ear compared to a steady flight in hover.

5.2 Future works

To complete this thesis, a set of recommendations for future research topics are proposed. A microphone array can be built in order to demonstrate the directivity of the drone noise. It would permit also to investigate deeper the broadband noise (over 2000 Hz) by improving the resolution in this zone.

Concerning the used empirical correlation for the Psychoacoustic Annoyance, its computation is based on aircraft noise and not on the drone's one. Therefore, it might not represent

the real human response since the nature of the drone noise is different. It should be interesting to take into account the exposure time as well as the varying frequencies so that the computation could reflect the real human perception of the drone noise. Also, further experimental data and other sound quality metrics will enhance the psychoacoustic annoyance interpretation.

A comparison with the evolution of the different Sound Quality Metrics could be performed with the aerodynamics of the quad-rotors in these diverse flight configurations.

By checking the spectra, the electric motor noise was present in higher frequencies. It should be interesting to verify if a correlation between the electric motor tone with the frequency variation of the BPF tone.

By the increase of the UAV in the world and for a lot of different uses, it could be curious also to compute the psychoacoustic and the noise annoyance for the wildlife. In fact, some animals need to be tracked in the savanna but they are afraid and annoyed by the drone noise. Therefore, understanding this psychoacoustic would lead to better nature.

Appendices

A Computation of the PSD and SPL with Welch's method

```python
#%% FUNCTION TO OBTAIN PSD AND SPL

# mic_data is the pressure recorded and divided by the microphone sensitivity for each microphone
# fs is the sampling frequency : fs = 51200 Hz
# win is the number of pressure data per segment

# The function returns f, PSD and SPL: the frequency corresponding to the Power Spectral Density (PSD) and to the Sound Pressure Level (SPL)

def spl(mic_data,fs, win):

    Press_mic = mic_data            # Pressure data registered of the microphones [Pa]
    n_fft=win*2                     # Length of the FFT used
    overlap=win/2                   # Number of points to overlap between segments

## signal.welch

    f, PSD = signal.welch(Press_mic, fs, window='hann', nperseg=win, noverlap=overlap, nfft=n_fft, detrend='constant', return_onesided=True, scaling = 'density', axis=-1, average='mean')

    SPL = np.zeros(len(PSD))
    for i in range (0,len(PSD)):
        SPL[i] = 10*math.log10( PSD[i] / (20*10**(-6))**2 )
    return f, PSD, SPL

win = 2**13

# Initialization of the array
psd = np.zeros ((4,3,win+1))
for i in range(4):
        psd[i,:,:] = spl(mic_data[i],fs,win)

# Plot of the SPL for the 4 microphones
plt.figure()
plt.loglog(psd[0,0,:],psd[0,2,:],'k',psd[1,0,:],psd[1,2,:],'b',psd[2,0,:],psd[2,2,:],'c',psd[3,0,:],psd[3,2,:],'r')
```

Data_Results/Python_Codes/SPLfunction.py

B Computation of the spectrogram

```python
#%% Computation and plot of the spectrogram for one microphone

# mic_data[0] takes the pressure data divided by the mic sensitivity of microphone 1
# fs is the sampling frequency = 51200 Hz
# noverlap is the number of points of overlap between blocks

# This function returns time: The times corresponding to midpoints of segments; powerSpectrum: Columns are the periodograms of successive segments; frequenciesFound: The frequencies corresponding to the rows in powerSpectrum.

n_fft=(2**13)*2  # Number of pressure data point for each block
powerSpectrum, frequenciesFound, time, imageAxis = plt.specgram(mic_data[0], NFFT=n_fft, mode='psd', Fs=fs, noverlap = 1000,scale = 'dB')

SpecSPLtmp = powerSpectrum / ((20*10**(-6))**2)
SpecSPL = 10*np.log10(SpecSPLtmp)

plt.figure()
plt.pcolormesh(time,frequenciesFound,SpecSPL,vmin = 0, vmax = 70,cmap = 'viridis',shading='gouraud')
```

Data_Results/Python_Codes/Spectrofunction.py

Bibliography

[1] A. W. Christian and R. Cabell. "Initial investigation into the psychoacoustic properties of small unmanned aerial system noise". In: *23rd AIAA/CEAS aeroacoustics conference*. 2017, p. 4051 (cit. on p. 1).

[2] A. J. Torija, R. H. Self, and J. L. Lawrence. "Psychoacoustic characterisation of a small fixed-pitch quadcopter". In: *INTER-NOISE and NOISE-CON Congress and Conference Proceedings*. Vol. 259. 8. Institute of Noise Control Engineering. 2019, pp. 1884–1894 (cit. on pp. 1, 2, 12, 42).

[3] D. Raya Islam, A. Stimpson, and M. Cummings. *Small UAV Noise Analysis*. Tech. rep. Tech. rep., Humans and Autonomy Laboratory, Durham, NC, USA, 2017 (cit. on p. 1).

[4] J.-P. Aurambout, K. Gkoumas, and B. Ciuffo. "Last mile delivery by drones: an estimation of viable market potential and access to citizens across European cities". In: *European Transport Research Review* 11.1 (2019), pp. 1–21 (cit. on p. 1).

[5] A. J. T. Martinez. "How to make noisy drones a little less irritating". In: (). https://researchoutreach.org/wp-content/uploads/2021/07/Antonio-J-Torija-Martinez.pdf (cit. on pp. 1, 2).

[6] J. Bergsma. "Drone in last mile delivery services". PhD thesis. 2021 (cit. on p. 1).

[7] B. Schäffer et al. "Drone Noise Emission Characteristics and Noise Effects on HumansA Systematic Review". In: *International Journal of Environmental Research and Public Health* 18.11 (2021) (cit. on pp. 2, 5).

[8] W. N. Alexander and J. Whelchel. "Flyover noise of multi-rotor sUAS". In: *INTER-NOISE and NOISE-CON Congress and Conference Proceedings*. Vol. 259. 7. Institute of Noise Control Engineering. 2019, pp. 2548–2558 (cit. on pp. 2, 28–30).

[9] P. Sijtsma, S. Oerlemans, and H. Holthusen. "Location of rotating sources by phased array measurements". In: *7th AIAA/CEAS Aeroacoustics Conference and Exhibit*. 2001, p. 2167 (cit. on p. 4).

[10] D. Y. Gwak, D. Han, and S. Lee. "Sound quality factors influencing annoyance from hovering UAV". In: *Journal of Sound and Vibration* 489 (2020) (cit. on p. 5).

[11] S. Cho et al. "Development of an automated wireless tension force estimation system for cable-stayed bridges". In: *Journal of Intelligent Material Systems and Structures* 21.3 (2010), pp. 361–376 (cit. on p. 6).

[12] C. Schram and M. Mendez. "Signal Processing course". en. In: *von Karman Institute of Fluid Dynamics* (2020) (cit. on p. 7).

[13] G. F. Coop. *MOSQITO*. Version 0.3.4. Nov. 2021. https://doi.org/10.5281/zenodo.5639403 (cit. on pp. 8, 38).

[14] A. N. S. I. C. on Bioacoustics. *American National Standard Psychoacoustical Terminology*. en. Google-Books-ID: 5Fo0GQAACAAJ. American National Standards Institute, 1973 (cit. on p. 9).

[15] *ISO 532-1:2017*. en. https://www.iso.org/cms/render/live/en/sites/isoorg/contents/data/standard/06/30/63077.html (visited on 12/12/2021) (cit. on p. 9).

[16] H. Fastl and E. Zwicker. *Psychoacoustics: Facts and Models*. English. 3rd edition. Berlin ; New York: Springer, Dec. 2006. ISBN: 978-3-540-23159-2 (cit. on pp. 9, 42).

[17] *Measurement Technique for the Simulation of the Auditory Sensation of Sharpness*. German. German Institute for Standardisation (Deutsches Institut für Normung). DIN: Berlin, Germany, Jan. 2009 (cit. on p. 9).

[18] P. Daniel and R. Weber. "Psychoacoustical roughness: Implementation of an optimized model". In: *Acta Acustica united with Acustica* 83.1 (1997), pp. 113–123 (cit. on p. 9).

[19] H. Fastl and E. Zwicker. "Sharpness and sensory pleasantness". In: *Psychoacoustics*. Springer, 2007, pp. 239–246 (cit. on p. 9).

[20] S. Glegg and W. Devenport. *Aeroacoustics of low Mach number flows: fundamentals, analysis, and measurement*. Academic Press, 2017. ISBN: 978-0-12-809651-2. DOI: 10.1017/aer.2018.128 (cit. on pp. 9–12).

[21] A. Filippone. "Aircraft noise prediction". In: *Progress in Aerospace Sciences* 68 (2014), pp. 27–63 (cit. on p. 10).

[22] M. Botre et al. "Validation of helicopter noise prediction system with flight data". In: *Vertical Flight Society 75th Annual Forum & Technology Display, Philadelphia, PA*. Vol. 13. 2019 (cit. on pp. 10, 11).

[23] *Explore HD Transparent PNGs & Cliparts, PngFind*. https://www.pngfind.com/ (visited on 12/09/2021) (cit. on pp. 11, 15, 18, 19).

[24] W. Cory. *Fans and ventilation: a practical guide*. Elsevier, 2010 (cit. on p. 11).

[25] *DJI 2312 Motor with CW Rotation for Phantom 2 Quadcopter | Walmart Canada*. https://www.walmart.ca/fr/ip/DJI-2312-Motor-with-CW-Rotation-for-Phantom-2-Quadcopter/PRD0X1PPOHJFWQV (visited on 12/19/2021) (cit. on p. 12).

[26] D. L. Huff and B. S. Henderson. "Electric Motor Noise for Small Quadcopters: Part 1 Acoustic Measurements". en. In: (June 2018). DOI: 10.2514/6.2018-2952. https://arc.aiaa.org/doi/10.2514/6.2018-2952 (visited on 10/21/2021) (cit. on p. 13).

[27] *Phantom 3 SE - Product Information - DJI*. en. https://www.dji.com/be/phantom-3-se/info (visited on 10/09/2021) (cit. on p. 14).

[28] *LabVIEW*. fr. https://www.ni.com/fr-be/shop/labview.html (visited on 11/05/2021) (cit. on pp. 15, 38).

[29] *GRAS 40PL-10 CCP Free-field Array Microphone, High Pressure*. da-dk. https://www.grasacoustics.com/products/special-microphone/array-microphones/product/831-gras-40pl-10-ccp-free-field-array-microphone-high-pressure (visited on 10/05/2021) (cit. on p. 16).

[30] *Calibrateur Acoustique | TYPE 4231| Brüel & Kjær*. fr. https://www.bksv.com/fr/transducers/acoustic/calibrators/sound-calibrator-4231 (visited on 12/22/2021) (cit. on p. 16).

[31] *Jet Aeroacoustic Facility for Aeronautical and Aerospace Research JAFAAR*. https://www.vki.ac.be/index.php/facilities-other-menu-148/aeroacoustics-facilities/58-research-and-consulting/facilities/aeroacoustics-facilities/84-anechoic-chamber-jaafar (visited on 12/07/2021) (cit. on p. 16).

[32] *PNG All*. en-US. https://www.pngall.com (visited on 12/09/2021) (cit. on p. 19).

[33] N. S. Zawodny, A. Christian, and R. Cabell. "A summary of NASA research exploring the acoustics of small unmanned aerial systems". In: (2018) (cit. on pp. 28, 31).

[34] S. O. Afari. "Prediction of noise associated with an isolated UAV propeller". MA thesis. Embry-Riddle Aeronautical University, 2019 (cit. on p. 28).

[35] Å. Skagerstrand, S. Köbler, and S. Stenfelt. "Loudness and annoyance of disturbing sounds–perception by normal hearing subjects". In: *International journal of audiology* 56.10 (2017), pp. 775–783 (cit. on pp. 32, 41, 42).

[36] A. Torija Martinez, Z. Li, et al. "Metrics for assessing the perception of drone noise". In: *Proceedings of Forum Acusticum 2020*. European Acoustics Association (EAA). 2020 (cit. on p. 37).

[37] I. Besnea. "Acoustic imaging and spectral analysis for assessing UAV noise". http://resolver.tudelft.nl/uuid:d4e37451-78d6-4b7d-bb34-721d04c176dc. MA thesis. Delft University of Technology, Apr. 2020 (cit. on pp. 37, 39, 42).

[38] *ArtemiS SUITE Software platform for sound and vibration analyses*. https://www.head-acoustics.com/products/analysis-software/artemis-suite (visited on 12/27/2021) (cit. on p. 38).